

**Submitted to *Transportation Science*
manuscript (Please, provide the manuscript number!)**

Authors are encouraged to submit new papers to INFORMS journals by means of a style file template, which includes the journal title. However, use of a template does not certify that the paper has been accepted for publication in the named journal. INFORMS journal templates are for the exclusive purpose of submitting to an INFORMS journal and should not be used to distribute the papers in print or online or to submit the papers to another publication.

Cooperative Adaptive Cruise Platoon Controller Design Considering Single Final String Stability and Control Switching

Hao Wang,Tiancheng Ruan,Zewen Zuo,Yuxuan Hou

School of Transportation, Southeast University, Nanjing 211189, P.R. China; Jiangsu Key Laboratory of Urban ITS, Southeast University, Nanjing, 210096, P.R. China; Jiangsu Province Collaborative Innovation Center of Modern Urban Traffic Technologies, Southeast University, Nanjing, 210096, P.R. China, {haowang@seu.edu.cn;ruantiancheng@seu.edu.cn; 220203312@seu.edu.cn;NOTEVENWRONG@outlook.com}

Rui Jiang

Key Laboratory of Transport Industry of Big Data Application Technologies for Comprehensive Transport, Ministry of Transport, Beijing Jiaotong University, Beijing, 100044, China, jiangrui@bjtu.edu.cn

With the development of Cooperative Adaptive Cruise Control (CACC) technology, CACC Market Penetration Rate (MPR) is expected to increase rapidly soon, resulting in more CACC platoons. However, the single vehicle control mode makes it difficult to take full advantage of the gain of CACC for capacity. Moreover, the platoon control model with a fixed platoon size is also ineffective since the size of the CACC platoon is arbitrary depending on the dispersion of CACCs and Manual Vehicles (MVs). Therefore, this paper first proposed a novel switching control mode — Cooperative Adaptive Cruise Platoon Control (CACPC)—that takes the CACC platoon as the control object to use CACC technology further. Secondly, a control switching method, Youla-Kučera (YK) parameterization, was adopted to ensure stability while switching the control modes for different platoon sizes. Finally, numerical analyses and simulations were conducted to explore the effectiveness of CACPC on dynamic performance. It is found that YK parameterization can significantly suppress the perturbation caused by the switching of control mode and maintain stability during the switching.

Key words: Cooperative adaptive cruise control; Platoon control; Single final string stability; Switching control.

History:

1. Introduction

To maintain safety, mobility, and environmental sustainability as transportation systems develop rapidly, Connected Autonomous Vehicle (CAV) technology has burgeoned and attracted considerable attention in the past decade. The connectivity and automation of the vehicle have been significantly improved. Vehicle-to-Infrastructure (V2I) communication technology guarantees partial or complete automation with the help of intra-vehicle sensors, and Vehicle-to-Vehicle (V2V) communication technology enables communication and cooperation between vehicles (Wang et al. 2019, Ploeg et al. 2011, Zhou et al. 2021).

The most typical application of V2V communication is Cooperative Adaptive Cruise Control (CACC). A vehicle controlled by this type of system automatically follows the preceding vehicles. Simulation results and field experiments reveal that, compared with traditional vehicles, cooperatively controlled CAVs can maintain a shorter time headway between vehicles. Therefore, consecutively connected vehicles can form a platoon-based driving mode through Cellular vehicle-to-everything (C-V2X) communication to improve traffic efficiency (Verizon North 2020, Gong and Du 2018, Wang et al. 2020). In extensive research, theoretical analyses and numerical simulations demonstrate that the CACC system is a more promising and attractive platooning technology in capacity, stability, safety, and pollutant emissions.

In the literature, various CACC control strategies have been developed, which can be divided into single-vehicle control and platoon control. As for the single-vehicle control, according to the literature (Qin, Wang, and Ran 2018, Ruan, Zhou, and Wang 2021), the primary goal of the single-vehicle control is to guarantee local stability, which means perturbations will be perturbations will gradually disappear over time. Moreover, most single-vehicle controllers are also designed to maintain the string stability, i.e., the disturbance propagates through the CACC and will not be amplified (Wang 2018, Sun, Zheng, and Sun 2018, Ploeg, Van De Wouw, and Nijmeijer 2013). According to research, string stability depends on the desired time gap adopted by CACC, which is inversely proportional to capacity. As the desired time gap gets smaller, string stability becomes harder to maintain (Navas, Milanés, and Nashashibi 2016). Thanks to the benefit of CACC on string stability, the desired time gap can be set lower while maintaining string stability as the CAV platoon size increases (Qin, Wang, and Ni 2021). However, for the case of single-vehicle control, guaranteeing the string stability of the CACC platoon by guaranteeing the string stability of each single CACC inevitably leads to much redundancy. Therefore, a control model that takes the string stability of the CACC platoon into account is needed to optimize the above-mentioned shortcomings.

On the other hand, the primary goal of the platoon control strategy is to coordinate the behaviors (accelerations or decelerations) of all of the following vehicles in the CAV platoon and optimize platoon control based on a specific objective function (Wang, Lu, and Peeta 2022, Shen, Kammara, and Du 2021, Xu et al. 2019). Wang et al. (Wang, Lu, and Peeta 2022) develop a robust cooperative control strategy to ensure the safe and efficient maneuvering of a CAV platoon in the worst-case situation due to the uncertainties in the vehicle dynamics. Shen et al. (Shen, Kammara, and Du 2021) propose a fully distributed optimization-based platoon-centred CAV platooning control via model predict control with a general prediction horizon. Numerical tests demonstrate the effectiveness of the proposed fully distributed schemes and CAV platooning control on transient traffic performance and string stability. Xu et al. (Xu et al. 2019) propose an energy-oriented robust platoon control strategy based on H_∞ method, which enables efficient driving of each vehicle while ensuring the platoon string stability.

While the aforementioned platoon control strategies can coordinate the car-following behaviors of CAVs in a platoon effectively, most of the platoon control strategies are stationary, i.e., the control strategy performs optimal control for a specific optimal objective after the CAV platoon is formed. Such platoon control

strategies can effectively improve the performance of the CAV platoon by improving the control objective. However, the design of platoon control strategy without paying attention to different CAV platoon sizes leads to its limitation by the platoon size and does not function properly when the platoon size changes. In addition, the platoon control strategies in existing research only focus on optimal control after the formation of the CAV platoon and ignore the platoon forming and splitting process. The process of controller switching can lead to strong autogenous perturbation, which is one of the factors of system insecurity (Stefanovic and Safonov 2008). Even if the controllers are stable before and after switching, they are not always stable during the switching process. Therefore, a switching control strategy that guarantees the stability of the CAV platoon under the switching process is needed to avoid the insecurity caused by platoon forming and splitting.

Moreover, it will take a long time for the CACC Market penetration rate (MPR) to grow due to the immaturity of CACC technology, as the CACC MPR is projected to be only 24.8% in 2045, according to the latest research (Bansal and Kockelman 2017). Therefore, there are heterogeneous traffic flows consisting of Manual Vehicles (MVs) and CACCs on the road. Since CACCs are separated into several CACC platoons with small platoon sizes by MVs, only a small amount of CACCs can guarantee that communication functions properly. Therefore, lots of CACCs will degrade into Adaptive Cruise Controls (ACCs) (Ruan et al. 2022, Yao et al. 2021). It is easy to ensure that CACCs maintain string stability by setting a proper desired time gap; however, it is challenging for ACCs (Montanino and Punzo 2021a, Shang and Stern 2021, Marsden, McDonald, and Brackstone 2001). ACCs do not gain string stability in traffic flow unless a large desired time gap is set, making single vehicle control mode ineffective. Fortunately, a platoon control mode that guarantees the string stability of the CACC platoon instead of the string stability of a single vehicle can balance the string stability and the capacity corresponding to the desired time gap.

Furthermore, limited by the slow growth of CACC MPRs, the platoon sizes of several CACC platoons separated by MVs are arbitrary, depending on the dispersion of CACCs and MVs on the road (Zhou et al. 2020). Therefore, the CACC platoon control mode with a fixed platoon size does not function effectively. To this end, a switchable CACC platoon control mode according to the platoon size is required to exploit the gain of CACC for traffic flow effectively.

In order to leverage the benefit of CACCs, this paper proposed a new decentralized switching control mode named Cooperative Adaptive Cruise Platoon Control (CACPC) that has taken the CACC platoon as the control object instead of a single vehicle. Firstly, we explored the combination of margin stable desired time gap under different platoon sizes based on string stability analyses. Secondly, Youla-Kučera (YK) parameterization was adopted to guarantee smoothness and stability in the control mode switching. Thirdly, a tuning function was proposed to ensure the application under different platoon sizes. Finally, the effectiveness of CACPC on dynamic performance was explored.

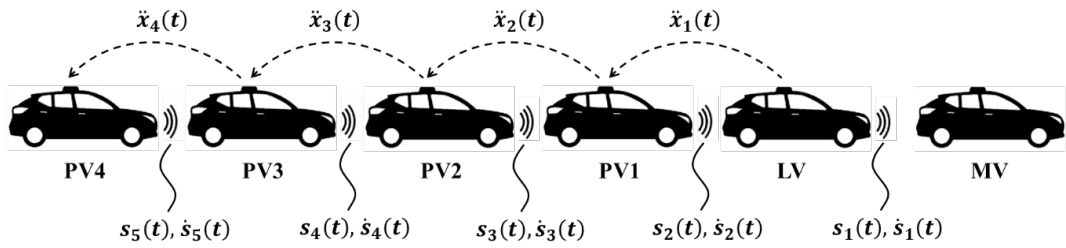


Figure 1 Schematic of CACC platoon.

The rest of this paper is organized as follows. Section 2 introduces the CACC system setup, control objectives, and control structure studied in this paper. Section 3 proposes the primary methodologies, including string stability analyses and YK parameterization. The theoretical results are presented in Section 4. Section 5 validates the theoretical results and explores the impact of CACPC. The conclusion is summarized in Section 6.

2. Problem Formulation

This section mainly introduces the background knowledge of the problems studied in this paper from three perspectives: CACC system setup, control objectives, and control structure.

2.1. CACC System Setup

Fig. 1 shows a schematic of the CACC platoon, where $s_i(t), \dot{s}_i(t)$ indicate the relative gap and relative velocity that CACC obtained through the onboard sensor, and $\ddot{x}_{i-1}(t)$ is the acceleration of the predecessor vehicle obtained through V2V communication.

The CACC design is based on a standard ACC system equipped with a communication module. A CACC platoon can be divided into a Lead Vehicle (LV) and $S - 1$ Platoon vehicles (PV)s based on the communication ability of the predecessor vehicle, where S denotes the maximum size of a CACC platoon. Notice that the CACC platoon cannot be infinitely long due to the limitation of the unreliable communication environment. Therefore, we assume the maximum platoon size is the platoon size that can keep communication functioning well. The LVs degrade to ACCs functionally because the predecessor vehicle is an ACC or MV, which cannot communicate, while the communication module of PVs is functioning (Dey et al. 2015, Navas and Milanés 2019).

Considering the feasibility of implementation, the controller used in this paper is a decentralized controller instead of a centralized one. The specific information flow topology (IFT) is predecessor following (PF) which means CACCs only communicate with the nearest predecessor to gain further information in advance. As for spacing policy, Constant Time Gap (CTG), including a constant part and a velocity-dependent part, is applied due to its widespread use.

2.2. String stability

We have considered the nuances in different definitions of string stability in the literature. In this paper, the single final string stability is adopted (Stüdli, Seron, and Middleton 2017). Namely, the perturbation only affects the lead vehicle and will not be amplified relative to the response of the last vehicle (Qin and Wang 2021, Montanino, Monteil, and Punzo 2021, Jin and Orosz 2014, Zhou et al. 2020, Wang 2018), i.e., between vehicle LV to vehicle PV4 (see Fig. 1). As for specific spacing policy, the error $e_i(t)$ between the desired and actual inter-vehicle gap is frequently considered in CTG to prevent collisions.

In this paper, the single final string stability of the CACC platoon is studied as a whole instead of analyzing each CACC in the platoon. To facilitate the analysis and focus on the amplification of perturbation, a frequency-domain approach is adopted to obtain a necessary and sufficient condition for the single final string stability of the CACC platoon, which will provide support for designing CACPC.

2.3. Control Structure

The CACC design is based on a standard ACC system and applies the most commonly used CTG policy. In this subsection, the control structures of the ACC and CACC system are discussed, respectively, in order to study the subsequent design of CACPC.

It is assumed that each CACC is equipped with i) an on-board radar responsible for collision detection via measuring the gap distance between any two consecutive vehicles, ii) a built-in GPS sensor for measuring the vehicular longitudinal position information, iii) a wireless on-board unit for communicating information of interest with its proximal vehicles via the C-V2X communication, iv) an upper-level controller for calculating the desired longitudinal acceleration based on the parameters obtained, and v) a lower-level controller for determining the throttle and brake actuator inputs so as to track the desired acceleration. Such an assumption is reasonable as the sensing, communication, and actuation units requested above are available in modern CAVs, and thus do not require specific changes in the existing vehicle configuration. Note that the on-board radar only functions when the CACC degrades to the ACC if communication is unavailable or malfunctioning since more accurate information can be obtained faster via communication.

Moreover, we remark that this paper only focuses on homogeneous CACCs where CACCs have the same control structure and controller parameters.

2.3.1. ACC Control Structure The primary control object of the ACC system is to maintain the desired gap from the preceding vehicle $s_{d,i}(t) = r_i + L_i + h_i \dot{x}_i(t)$, including a velocity-dependent part and a constant part, where L_i represents the vehicle length, r_i is the standstill distance, x_i denotes the longitudinal position of vehicle i and h_i represents the desired time gap of vehicle i . Using the onboard sensor, the relative gap $s_i(t) = x_{i-1}(t) - x_i(t)$ and relative velocity $\dot{s}_i(t)$ are measured. In a standard ACC system, the feedback controller controls the error $e_i(t) = s_i(t) - s_{d,i}(t)$ between the desire gap and relative gap.

The ACC control structure is schematically depicted in Fig. 2 (a).

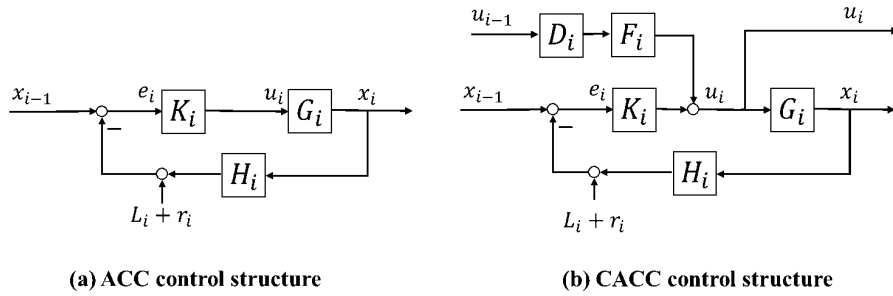


Figure 2 Control structure of ACC and CACC: (a) ACC; (b) CACC.

As shown in Fig. 2 (a), the ACC control structure is represented as a system construction drawing with vehicle position as input and output. The model $K_i(s)$ is the ACC feedback gain, which can be given as:

$$K_i(s) = k_p + k_d s, \quad (1)$$

where k_p is error gain and k_d is error speed gain, the specific parameter setting is based on previous research (Milanés and Shladover 2014, Milanés et al. 2013).

The model $G_i(s)$ represents a lower level controller longitudinal vehicle dynamics, where the input $u_i(t)$ of $G_i(s)$ is the desired acceleration derived from $K_i(s)$ and the output $x_i(t)$ is the output position based on the control loop to track desired acceleration through actuation of the throttle and brake system. The linear transfer function of $G_i(s)$ can be represented by (Ploeg, Van De Wouw, and Nijmeijer 2013):

$$G_i(s) = \frac{k_G}{s^2(\tau_i s + 1)} e^{-\phi_i s}, \quad (2)$$

where $\tau_i^{-1} = \omega_{bw,l,i}$ is the closed-loop bandwidth, k_G is the model gain and ϕ_i is the time delay of vehicle actuator and intra-vehicle communication, the specific parameter setting is shown in Table. 1.

Model $H_i(s)$ is the ACC feedback gain, which can be given as:

$$H_i(s) = 1 + h_i s, \quad (3)$$

where h_i is the desired time gap of vehicle i.

The closed-loop transfer function of the ACC system in the frequency domain is as follows:

$$\mathcal{J}_{i,ACC}(s) = \frac{X_i(s)}{X_{i-1}(s)} = \frac{G_i(s)K_i(s)}{1 + H_i(s)G_i(s)K_i(s)}, \quad (4)$$

where $X_i(s)$ is the Laplace transform of $x_i(t)$.

2.3.2. CACC Control Structure As discussed above, the CACC controller is equipped with a communication module that extends the standard ACC feedback controller. The specific control structure is schematically depicted in Fig. 2 (b).

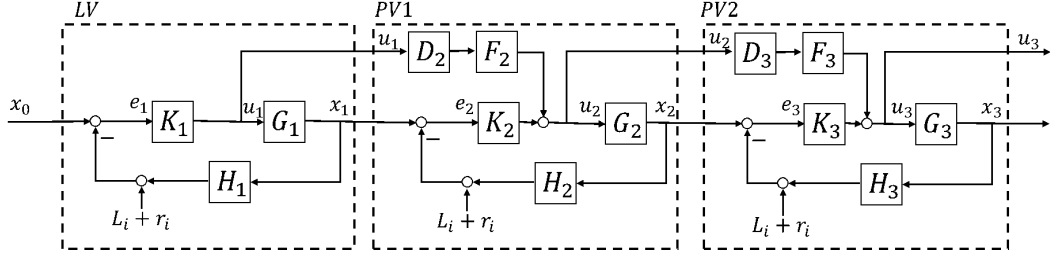


Figure 3 CACPC structure.

For simplicity, the definitions of model $H_i(s)$, $G_i(s)$, and $K_i(s)$ in system construction drawing are omitted because they are the same as those in Section. 2.3.1. The acceleration $\ddot{x}_{i-1}(t)$ of the predecessor vehicle obtained through V2V communication is used as a feedforward control signal through the feedforward filter $F_i(s)$ and the communication delay model $D_i(s)$.

The model $D_i(s)$ is directly related to the constant communication delay θ_i , which can be expressed as:

$$D_i(s) = e^{-\theta_i s}, * \quad (5)$$

where θ_i represents the constant communication delay. The specific parameter setting is according to previous research (Navas, Milanés, and Nashashibi 2016, Zhang et al. 2020).

The model $F_i(s)$ is the communication feedforward filter which can be given as:

$$F_i(s) = (H_i(s)G_i(s))^{-1}. \quad (6)$$

The closed-loop transfer function of the CACC system in the frequency domain is as follows:

$$\mathcal{J}_{i,CACC}(s) = \frac{X_i(s)}{X_{i-1}(s)} = \frac{(K_i(s) + D_i(s)F_i(s))G_i(s)}{1 + H_i(s)G_i(s)K_i(s)}. \quad (7)$$

2.3.3. CACPC structure As the control system for the controller design in this paper, the CACC platoon is designated as the primary control unit for string stability analyses. We can couple the control structure of ACC and CACC by merging the inner and outer signals, thus establishing the structure of CACPC. The specific structure of the CACPC is schematically depicted in Fig. 3.

For simplicity, the definitions of model $H_i(s)$, $G_i(s)$, $K_i(s)$ and $D_i(s)$ in system construction drawing are omitted because they are the same as those in Section. 2.3.1 and 2.3.2.

The closed-loop transfer function of CACPC system in the frequency domain is as follows:

$$\begin{aligned} \mathcal{J}_{\text{platoon}}(s) &= \frac{X_n(s)}{X_0(s)} = \frac{X_n(s)}{X_{n-1}(s)} \frac{X_{n-1}(s)}{X_{n-2}(s)} \cdots \frac{X_1(s)}{X_0(s)} \\ &= \mathcal{J}_{1,ACC}(s) \prod_{i=2}^n \mathcal{J}_{i,CACC}(s), \end{aligned} \quad (8)$$

where n denotes the platoon size.

3. Methodology

In this section, the primary methodology applied in this paper is introduced, including the transfer function method for string stability analyses and the YK parameterization for controller switching.

3.1. String stability analysis

Laplace transform is a classic method to explore string stability in a direct and precise manner. Moreover, it has been adopted in extensive research (Orosz, Moehlis, and Bullo 2011, Montanino and Punzo 2021b, Feng et al. 2019). Therefore, single final string stability analyses of this paper are conducted based on the Laplace transform. The relationship of the perturbation propagating through the CACC platoon in the frequency domain is:

$$\mathcal{J}_{\text{platoon}}(s) = \frac{X_n(s)}{X_0(s)}. \quad (9)$$

According to the definition of string stability, a sufficient and necessary conservative condition for string stability can be derived according to the \mathcal{L}_∞ norm:

$$\|x_n(t)\|_{\mathcal{L}_\infty} \leq \|x_0(t)\|_{\mathcal{L}_\infty} \quad (10)$$

where $x_n(t)$ and $x_0(t)$ are the inverse Laplace transformation of $X_n(s)$ and $X_0(s)$, respectively; $\|\cdot\|_{\mathcal{L}_\infty}$ is the \mathcal{L}_∞ norm, which deals with the peak of perturbations.

Moreover, according to the relationship $\|g\|_1 = \sup_{x \in L_\infty} \frac{\|y\|_{\mathcal{L}_\infty}}{\|x\|_{\mathcal{L}_\infty}}$ Equation(10) can be replaced as:

$$\|j(t)\|_1 \leq 1 \quad (11)$$

where $j(t)$ denotes the impulse response of $\mathcal{J}_{\text{platoon}}(s)$.

Furthermore, the Equation(11) can be replaced by the following two conditions (Swaroop 1994):

$$\|\mathcal{J}_{\text{platoon}}(s)\|_\infty \leq 1 \quad \& \quad j(t) > 0 \quad (12)$$

We remark that we adopt \mathcal{L}_∞ norms of the string stability instead of \mathcal{L}_2 norms. Although \mathcal{L}_2 norms can provide more explicit derivation, it only deals with the energy dissipation in the upstream direction and not the peak of perturbations (Darbha 2003). In addition, the single final string stability is adopted in this paper for string stability analyses since it can deal with the relationship between peaks of perturbation before and after it spreads over the platoon. So that the string stability indicates the perturbation is not amplified by the CACC platoon (Stüdli, Seron, and Middleton 2017).

3.2. Controller switching method: Youla-Kucera parametrization

Although the controllers are designed to maintain string stability of platoon under different platoon sizes, the switching of the controllers will cause perturbations inevitably, which will cause safety hazards in the traffic flow. Therefore, a parameterization method for smooth switching between different controllers is needed to ensure the feasibility of the above CACC controllers design.

Youla-Kucera (YK) parametrization is a method to stabilize the class of a given plant that contains all stabilizing controllers (Dasgupta and Anderson 1996, Navas, Milanés, and Nashashibi 2017). One of the advantages of this method is that the performance transfer function is tuned with a particular parameter, which means that the stability of unstable open-loop controllers can be maintained while switching between controllers.

3.2.1. Fundamentals on YK parametrization The basis of YK parametrization is described in detail below, which includes doubly coprime factorization and YK parameterization of all stabilizing controllers.

Basic notations are introduced below. $\mathbb{R}H_\infty$ is the real stable transfer function space; G and K_i maintain the same definitions as in Section 3.

For applying YK parametrization, the internal dynamics of the vehicles G need to be presented as state-space representation:

$$\begin{aligned}\dot{m}(t) &= Am(t) + Bu(t), \\ x(t) &= Cm(t) + Du(t)\end{aligned}, G(s) = \begin{bmatrix} A & B \\ C & D \end{bmatrix}, \quad (13)$$

where t indicates time, $m(t)$ is the state vector, $\dot{m}(t)$ is the evolution of the state vector over time, $x(t)$ is the output vector, and $u(t)$ is the control vector. A , B , C , and D are the constant coefficients matrices of state-space matrices of G .

Any appropriate controller K_i could stabilize this system, which is represented as:

$$\begin{aligned}\dot{n}(t) &= A_i^c n(t) + B_i^c e(t), \\ u(t) &= C_i^c n(t) + D_i^c e(t)\end{aligned}, K_i(s) = \begin{bmatrix} A_i^c & B_i^c \\ C_i^c & D_i^c \end{bmatrix}, \quad (14)$$

where $n(t)$ is the state vector, and A_i^c, B_i^c, C_i^c and D_i^c are the constant coefficients matrices of state-space matrices of K_i . It should be noted that K_0 represents the initial controller, and K_1 represents the controller after a complete switch, thanks to YK parametrization.

3.2.2. Doubly coprime factorization Factorization means the plant and controllers are represented as the products of two transfer functions. coprimeness refers to the absence of common zeros in the right half-plane, and double coprimeness excludes unstable pole/zero cancellations and refers to the idea of being right and left coprime.

The coprime factors of G and K_i can be expressed as:

$$G = NM^{-1} = \tilde{M}^{-1}\tilde{N}, K_i = U_i V_i^{-1} = \tilde{V}_i^{-1}\tilde{U}_i, \quad (15)$$

where coprime factors $N, M, \tilde{M}, \tilde{N}, U_i, V_i, \tilde{U}_i, \tilde{V}_i \in \mathbb{R}H_\infty$ satisfy double Bezout's identity (Pommaret and Quadrat 1998):

$$\begin{aligned}\begin{bmatrix} \tilde{V}_i & -\tilde{U}_i \\ -\tilde{N} & \tilde{M} \end{bmatrix} \begin{bmatrix} M & U_i \\ N & V_i \end{bmatrix} &= \begin{bmatrix} M & U_i \\ N & V_i \end{bmatrix} \begin{bmatrix} \tilde{V}_i & -\tilde{U}_i \\ -\tilde{N} & \tilde{M} \end{bmatrix} \\ &= \begin{bmatrix} I & 0 \\ 0 & I \end{bmatrix}.\end{aligned} \quad (16)$$

Using the relationship of state-space representation and transfer function $G(s) = C(sI - A)^{-1}B$ and $K_i(s) = C_i^c(sI - A_i^c)^{-1}B_i^c + D_i^c$, coprime factors can be derived by:

$$\begin{bmatrix} M & U_i \\ N & V_i \end{bmatrix} = \left[\begin{array}{cc|cc} A + BF & 0 & -B & 0 \\ 0 & A_i^c + B_i^c F_i^c & 0 & B_i^c \\ -F & C_i^c + D_i^c F_i^c & I & D_i^c \\ -C & F_i^c & 0 & I \end{array} \right], \quad (17)$$

$$\begin{bmatrix} \tilde{V}_i & -\tilde{U}_i \\ -\tilde{N} & \tilde{M} \end{bmatrix} = \left[\begin{array}{cc|cc} A + BD_i^c C & BC_i^c & -B & BD_i^c \\ B_i^c C & A_i^c & 0 & B_i^c \\ F_i - D_i^c C & -C_i^c & I & -D_i^c \\ C & -F_i^c & 0 & I \end{array} \right], \quad (18)$$

where F and F_i^c should be chosen such that $A + BF, A_i^c + B_i^c F_i^c \in \mathbb{R}H_\infty$. Straight lines indicate the elements of the matrix that belong to each factor, respectively. The proof of the Equation (17-18) is detailed in Appendix B.

During the process of controller switching, only the vehicle decision controller K_i from K_0 switches to K_1 and internal dynamics of the vehicles G remain unchanged, which means M and N remain unchanged while U_0, V_0 are converted to U_1, V_1 .

3.2.3. YK parameterization of all stabilizing controllers The fundamental of YK parametrization is the initial interpolation controller with a parameter Q to obtain all controllers K that can stabilize a given plant G . The expression of $K(Q)$ and Q is described as:

$$\begin{aligned} K(Q) &= (U_0 + M\gamma Q)(V_0 + N\gamma Q)^{-1} \\ &= (\tilde{V}_0 + \gamma Q\tilde{N})^{-1}(\tilde{U}_0 + \gamma Q\tilde{M}), Q \in \mathbb{R}H_\infty^{p \times m}, \end{aligned} \quad (19)$$

$$Q = \tilde{U}_1 - \tilde{V}_1 \tilde{V}_0^{-1} \tilde{U}_0, \quad (20)$$

where $\gamma \in [0, 1]$ is a scalar factor playing a pivotal role as a switching signal in controller interpolation, indicating the level of interconnection of the two controllers (Niemann and Stoustrup 1999). When $\gamma = 0$, the controller is completely taken over by K_0 , while K_1 is fully controlled when $\gamma = 1$.

Proof: First, check the matrix of the closed-loop feedback control system.

$$\begin{aligned}
& \begin{bmatrix} I & -K(Q) \\ -G & I \end{bmatrix}^{-1} \\
&= \begin{bmatrix} I & -(\tilde{V}_0 + \gamma Q \tilde{N})^{-1}(\tilde{U}_0 + \gamma Q \tilde{M}) \\ -\tilde{M}^{-1} \tilde{N} & I \end{bmatrix}^{-1} \\
&= \left\{ \begin{bmatrix} (\tilde{V}_0 + \gamma Q \tilde{N})^{-1} & 0 \\ 0 & \tilde{M}^{-1} \end{bmatrix} \begin{bmatrix} \tilde{V}_0 + \gamma Q \tilde{N} & -(\tilde{U}_0 + \gamma Q \tilde{M}) \\ -\tilde{N} & \tilde{M} \end{bmatrix} \right\}^{-1} \\
&= \begin{bmatrix} M & U_0 + M\gamma Q \\ N & V_0 + N\gamma Q \end{bmatrix} \begin{bmatrix} \tilde{V}_0 + \gamma Q \tilde{N} & 0 \\ 0 & \tilde{M} \end{bmatrix} \\
&= \left\{ \begin{bmatrix} M & U \\ N & V \end{bmatrix} + \begin{bmatrix} 0 & \gamma M Q \\ 0 & \gamma N Q \end{bmatrix} \right\} \left\{ \begin{bmatrix} \tilde{V} & 0 \\ 0 & \tilde{M} \end{bmatrix} + \begin{bmatrix} \gamma Q \tilde{N} & 0 \\ 0 & 0 \end{bmatrix} \right\}^{-1} \\
&= \begin{bmatrix} M & U \\ N & V \end{bmatrix} \begin{bmatrix} \tilde{V} & 0 \\ 0 & \tilde{M} \end{bmatrix} + \begin{bmatrix} \gamma M Q \tilde{N} & 0 \\ \gamma N Q \tilde{N} & 0 \end{bmatrix} + \begin{bmatrix} 0 & \gamma M Q \tilde{M} \\ 0 & \gamma N Q \tilde{M} \end{bmatrix} \\
&= \begin{bmatrix} \tilde{V} & -\tilde{U} \\ -\tilde{N} & \tilde{M} \end{bmatrix}^{-1} \begin{bmatrix} \tilde{V}^{-1} & 0 \\ 0 & \tilde{M}^{-1} \end{bmatrix}^{-1} + \begin{bmatrix} \gamma M Q \tilde{N} & \gamma M Q \tilde{M} \\ \gamma N Q \tilde{N} & \gamma N Q \tilde{M} \end{bmatrix} \\
&= \begin{bmatrix} M & U \\ N & V \end{bmatrix} \begin{bmatrix} \tilde{V} & 0 \\ 0 & \tilde{M} \end{bmatrix} + \begin{bmatrix} M \\ N \end{bmatrix} \gamma Q \begin{bmatrix} \tilde{N} & \tilde{M} \end{bmatrix} \\
&= \begin{bmatrix} I & -K \\ -G & I \end{bmatrix}^{-1} + \begin{bmatrix} M \\ N \end{bmatrix} \gamma Q \begin{bmatrix} \tilde{N} & \tilde{M} \end{bmatrix} \in \mathbb{R}H_{\infty}^{p,xm}.
\end{aligned} \tag{21}$$

From Equation (21), it is clearly that any controller $K(Q)$ parameterized by $Q \in \mathbb{R}H_{\infty}^{p,xm}$ stabilizes the plant G according to the Corollary 4.2 in references (Tay, Mareels, and Moore 1998, Mahtout et al. 2020).

The closed-loop poles of the system during the switching process are the combination of $[G, K_0]$ and $[G, K_1]$, which can maintain the stability of the system under any combination of Q and γ , thus ensuring the stable switch of the controllers independent of γ (Niemann and Stoustrup 1999).

4. Theoretical analyses

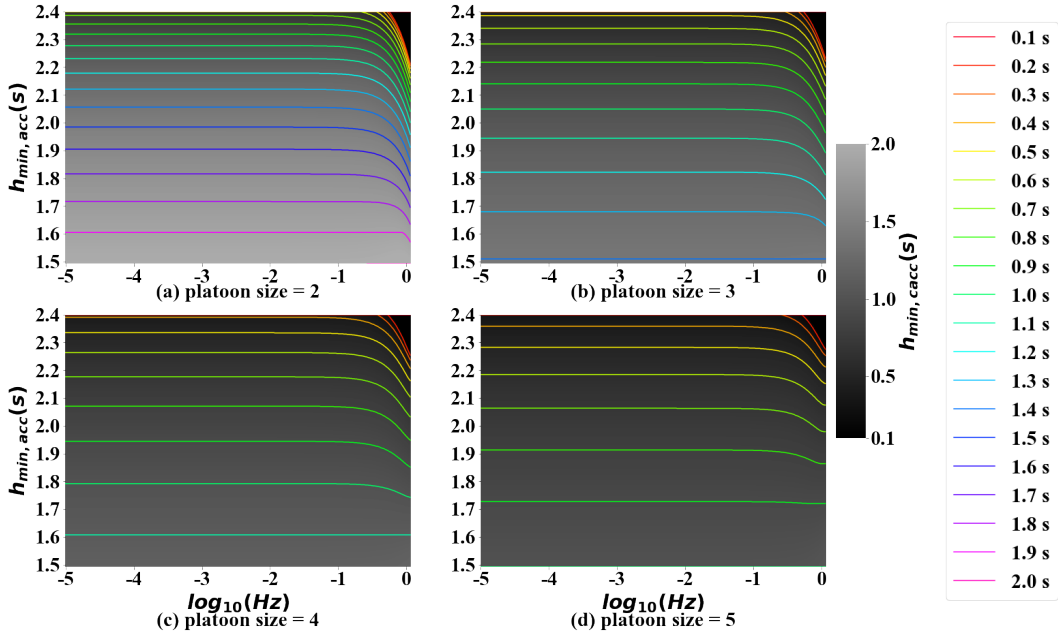
In this section, the detailed controller design process is carried out using the methodology proposed in Section 3. The process includes selecting the best desired time gap strategy for ACC and CACC in the case of the CACC platoon, determining the YK parameter in the controller switching of ACC and CACC, and deciding γ function. In addition, to facilitate subsequent calculations and experiments, the above-defined controller coefficients selected in this paper are as follows, which are set based on existing research (Milanés and Shladover 2014, Milanés et al. 2013, Navas, Milanés, and Nashashibi 2016) and field experiments employed detailed in Appendix A. Moreover, the maximum platoon size S of the CACC platoon is set to 5 in the paper, which is absolutely feasible and effective for communication latency and packet loss rates from the perspective of the communication technology.

4.1. Analyses of string stability

When the CACC platoon is formed, taking the CACC platoon as the control object can maintain a smaller desired time gap without losing string stability. In order to explore the minimum desired time gap combi-

Table 1 Parameters chosen for ACC and CACC controller.

Parameter	k_p	k_d	τ_i	k_G	ϕ_i	θ_i
Value	0.45 s ⁻²	0.25 s ⁻¹	0.7862 s/rad	0.9403	0.2 s.	0.3 s

**Figure 4** Contour plot of perturbation frequency versus $h_{\min,acc}$, indicating the corresponding minimal value for $h_{\min,cacc}$.

nation for the CACC platoon, the theoretical analyses regarding string stability are carried out using the method proposed in Section 3.1.

As for the desired time gap $h_i = h_{i,min}$, margin string stability criterion (12) is met, and string stability can be guaranteed when $h_i \geq h_{i,min}$ (Naus et al. 2010). However, due to the complexity of the CACPC structure, the calculation of the minimum desired time gap $h_{i,min}$ is too complicated and cannot give an algebraic equation of h_{acc} and h_{cacc} , so the derivation is not discussed here. A numerical approximation approach is adopted to explore the combination of $h_{\min,acc}$ and $h_{\min,cacc}$ as margin string stable according to Equation (12). Moreover, since the perturbation faced in real traffic conditions is considered to be of infinite wavelength (Bian et al. 2019, Xiao and Gao 2011), we only focus on the magnitude of the transfer function under low frequency ($10^{-5} - 10^0$ Hz) (Oncu et al. 2014). Fig. 4 shows that $h_{\min,cacc}$ changes with $h_{\min,acc}$ over different frequencies where the heatmap shows the margin stable combination of $h_{\min,cacc}$ and $h_{\min,acc}$ under different $h_{\min,acc}$ and perturbation frequency.

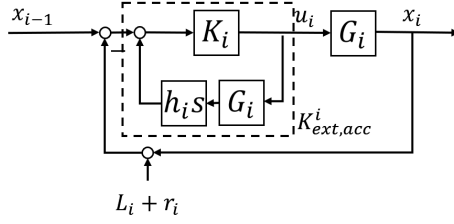


Figure 5 Equivalent ACC control structure.

It can be clearly found in Fig. 4 that CACC can maintain a smaller desired time gap with platoon size increasing. Moreover, $h_{min,cacc}$ can significantly decrease with $h_{min,acc}$ increasing, which means the feasibility of eliminating the redundancy within the CACC platoon through the appropriate deployment of the desired time gap. In addition, string stability can be significantly improved as the frequency of perturbation approaches 10^0 Hz, which is represented as the arc under $10^{-0.5} - 10^0$ Hz in Fig. 4. When we focus on the region of $10^{-5} - 10^{-0.5}$ Hz, an interesting phenomenon is discovered that $h_{min,cacc}$ stays the same as the frequency increases, which means the combination of $h_{min,cacc}$ and $h_{min,acc}$ to guarantee the string stability is determined for a specific platoon size.

Based on the conclusions obtained above, in order to maximize the capacity while ensuring string stability and safety, we choose $h_{1,acc} = 2s$ and $h_{1,cacc} = 0.4s$ for the case of $S = 5$ while the desired time gap settings of ACC and CACC for the case of $S = 2$ are $h_{0,acc} = 2.108s$ and $h_{0,cacc} = 0.747s$ in this paper.

4.2. Analyses of controller switching

For the LV in a CACC platoon, since it cannot communicate with the predecessor vehicle, it loses the information gain from the communication module, so its control system is represented by standard ACC, as shown in Fig. 2 (a).

4.2.1. Modify ACC controller To incorporate the desired time gap into the controller, the ACC controller in Fig. 2 (a) is reconstructed so that the ACC controller can perform stable interpolation for the different desired time gaps h_i . Moreover, the corresponding equivalent ACC control structure is shown in Fig. 5. The transfer function of the extended controller is as follows:

$$K_{ext,acc}^i(s) = \frac{K_i}{1 + h_i G_i K_i s}. \quad (22)$$

4.2.2. YK parametrization for ACC controller Based on the mathematical basis introduced in Section. 3.2, the control structure applied to controller switching needs to be modified accordingly by introducing a dual coprime factor. The control structure for switching based on left coprime factors is shown in Fig. 6:

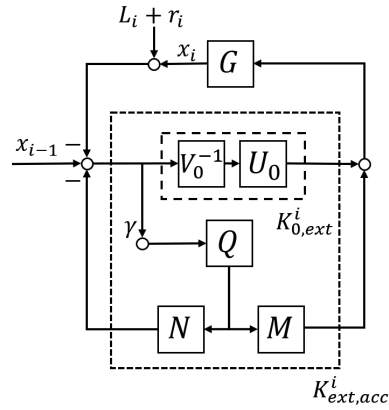


Figure 6 YK control structure for ACC controllers switching.

For stable switching purposes, coprime factors need to meet double Bezout's identity as shown in Equation (16) based on the state-space matrix of transfer functions of $K_{0,acc}$, $K_{1,acc}$. The specific transfer functions of coprime factors are as follows:

$$\begin{aligned} U_0 &= \frac{-s(s+1.272)(s+1.8)}{(s+4.42)(s^2+1.836s+1.027)}, \\ V_0 &= \frac{-4(s^2+1.902s+1.135)}{(s+4.42)(s^2+1.836s+1.027)}, \\ U_1 &= \frac{-s(s+1.272)(s+1.8)}{(s+4.42)(s^2+1.808s+0.9741)}, \\ V_1 &= \frac{-4(s^2+1.87s+1.076)}{(s+4.42)(s^2+1.808s+0.9741)}. \end{aligned} \quad (23)$$

As for the YK parameter Q_{acc} , substitute coprime factors into Equation(20):

$$Q_{acc} = \frac{-0.1005(s+1.892)(s+4.38)(s+4.42)}{(s+4.42)^3(s^2+1.808s+0.9741)(s^2+1.836s+1.027)^2}. \quad (24)$$

4.2.3. Modify CACC controller Similar to the method adopted in Section 4.2.1, the system construction drawing of the CACC controller is in Fig. 3, which is reconstructed to incorporate the desired time gap h_i into the controller. Furthermore, the corresponding equivalent CACC control structure is shown in Fig. 7. The transfer function of the extended controller is as follows:

$$K_{ext,cacc}^i(s) = \frac{K_i}{1 + h_i G_i K_i s}. \quad (25)$$

4.2.4. YK parametrization for CACC controller Similar to Section 4.2.2, the control structure applied to controller switching needs to be modified accordingly by introducing a dual coprime factor based on the mathematical basis presented in Section 3.2. The control structure for switching based on left coprime factors is shown in Fig. 8:

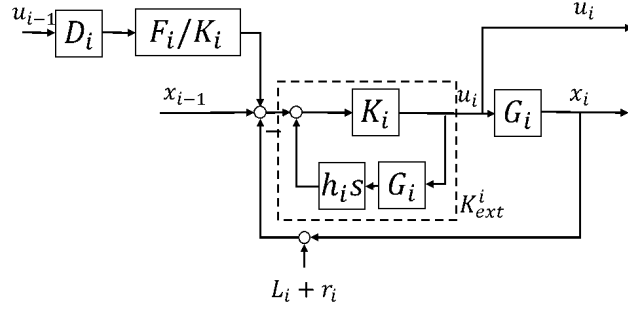


Figure 7 Equivalent CACC control structure.

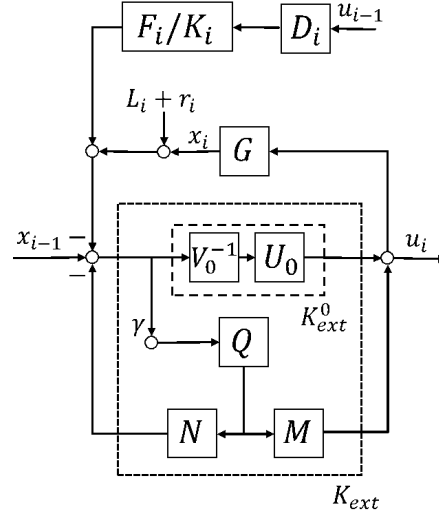


Figure 8 YK control structure for CACC controllers switching.

Based on Equation (17-18), coprime factors which meet double Bezout's identity, as shown in Equation (16), can be obtained easily. The specific transfer functions of coprime factors are as follows:

$$\begin{aligned}
U_3 &= \frac{-s(s+1.272)(s+1.8)}{(s+4.406)(s+1.159)(s+0.3148)}, \\
V_3 &= \frac{-4(s+1.144)(s+0.3515)}{(s+4.406)(s+1.159)(s+0.3148)}, \\
U_4 &= \frac{-s(s+1.272)(s+1.8)}{(s+4.397)(s+1.226)(s+0.1438)}, \\
V_4 &= \frac{-4(s+1.221)(s+0.1587)}{(s+4.397)(s+1.226)(s+0.1438)}.
\end{aligned} \tag{26}$$

As for the YK parameter Q_{cacc} , substitute coprime factors into Equation(20):

$$Q_{cacc} = \frac{-0.4451(s+4.402)(s+3.51)(s+1.918)(s+1.8)}{\frac{(s+1.274)(s+1.219)(s+1.414)(s+0.3596)(s+0.1572)}{(s+4.397)(s+1.8)(s+1.272)(s+1.226)(s+0.1438)}}. \tag{27}$$

4.3. Tuning function γ for CACC platoon

The theoretical results of Section 4.1 point out that different CACC platoon sizes have different combinations of $h_{min,acc}$ and $h_{min,cacc}$ as string stability margin. To avoid being restricted by the platoon size, a corresponding tuning function γ for the platoon size is required so that CACPC can be applied under different platoon sizes.

The theoretical results of Section 4.1 indicate that different CACC platoon sizes have different combinations of $h_{min,acc}$ and $h_{min,cacc}$ as string stability margin. In order to avoid being restricted by the platoon size, the corresponding tuning function γ about platoon size is required so that CACPC can be applied under different platoon sizes. Based on the reasons above, a numerical analysis is conducted to obtain the combination of γ_{acc} and γ_{cacc} , which can maintain the string stability of the CACC platoon under different platoon sizes. The results are shown in Fig. 9, where the transparent grey planes represent the string stability margin planes, and the colored surfaces indicate the amplitudes under different $gamma_{acc}$ and $gamma_{cacc}$. Moreover, the black curves denote the intersections of the string stability margin plane and the amplitude surface, which are the margin stable combinations of γ_{acc} and $gamma_{cacc}$. It is worth noting that Fig. 9 is carried out at the frequency of 10^{-5} Hz, and further exploration that covers a broader frequency domain is carried out in Section 5.1.

We can conclude from Fig. 9 that the intersection of the transparent plane and string stability's surface is the basis for selecting γ_{acc} and γ_{cacc} , which can ensure string stability and tap the advantages of CACPC as much as possible. Through the curve-fitting method, we can get the expression of the intersection as follows (since any γ can meet the string stability at platoon size = 5, there is no corresponding expression.):

$$\gamma_{cacc} = \begin{cases} -0.0501 * \gamma_{acc} + 0.2221, & \text{if } n = 2 \\ -0.0248 * \gamma_{acc} + 0.5815, & \text{if } n = 3 \\ -0.0165 * \gamma_{acc} + 0.8995, & \text{if } n = 4 \end{cases} \quad (28)$$

Considering the gain-scheduling method, the appropriate tuning function γ is derived based on the expression above:

$$\gamma_{acc} = \begin{cases} 0, & \text{if } n = 1 \\ 0.4, & \text{if } n = 2 \\ 0.7, & \text{if } n = 3 \\ 0.9, & \text{if } n = 4 \\ 1, & \text{if } n = 5 \end{cases}, \quad (29)$$

$$\gamma_{cacc} = \begin{cases} 0, & \text{if } n = 1 \\ 0.3, & \text{if } n = 2 \\ 0.6, & \text{if } n = 3 \\ 0.9, & \text{if } n = 4 \\ 1, & \text{if } n = 5 \end{cases}, \quad (30)$$

where n denotes platoon size.

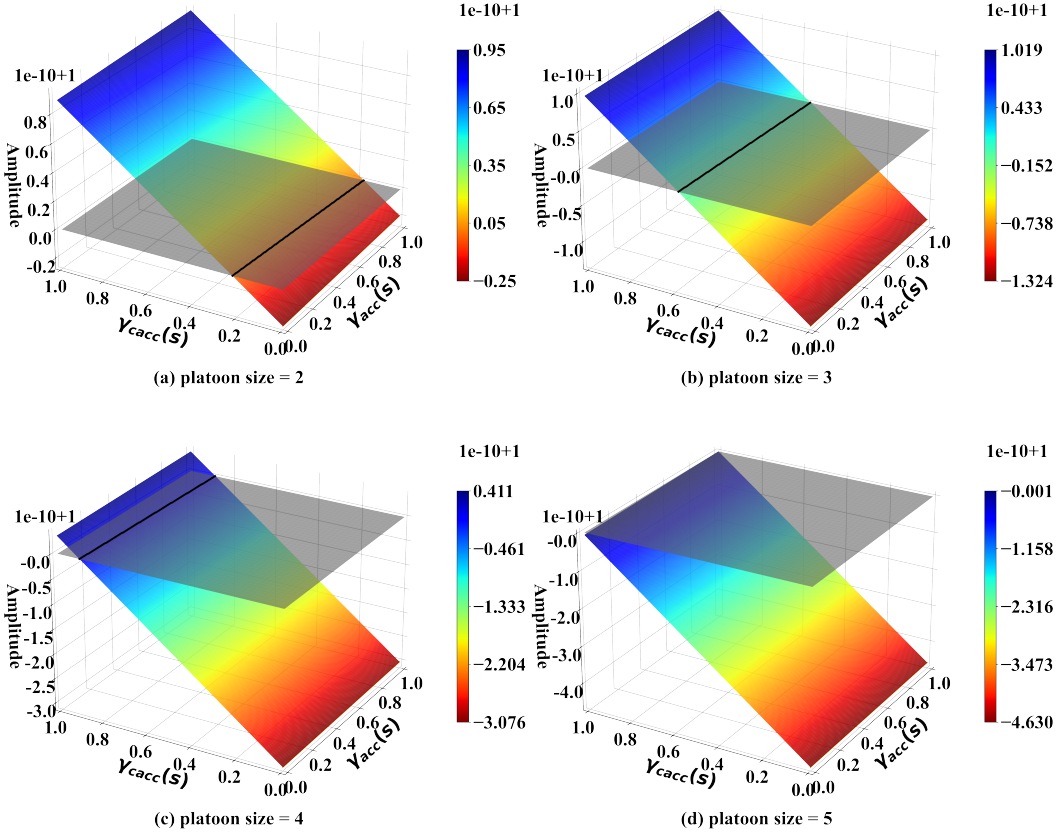


Figure 9 String stability's surface depending on YK γ_{acc} and $\gamma_{cacc}*$.

5. Numerical analyses

In this section, we first validate the string stability of CACPC based on the theoretical result derived in Section. 4 by numerical simulation. Then a series of simulation experiments are conducted to explore the impact of YK parameterization on dynamic performance.

5.1. Validation of string stability

Based on the results in Section. 4.2 and 4.3, we have obtained the amplitude of CACPC under different platoon sizes. It is necessary to keep the string stable to prevent the perturbation from being amplified during propagation. Therefore, a numerical experiment is conducted to explore the string stability of the CACC platoon under low frequency ($10^{-5} - 10^0$ Hz). Fig. 10 shows the result where the curved surface represents the amplitude of the CACC platoon under low frequency ($10^{-5} - 10^0$ Hz) and different platoon sizes.

Fig. 10 indicates that the CACPC proposed above can avoid amplifying perturbation, which means it can maintain string stability during the switching process.

5.2. Simulation experiments of YK parameterization

Unlike theoretical analyses, behaviors observed in simulation experiments are closer to those in the real traffic environment. In order to further explore the actual effect of the controller switching using the YK

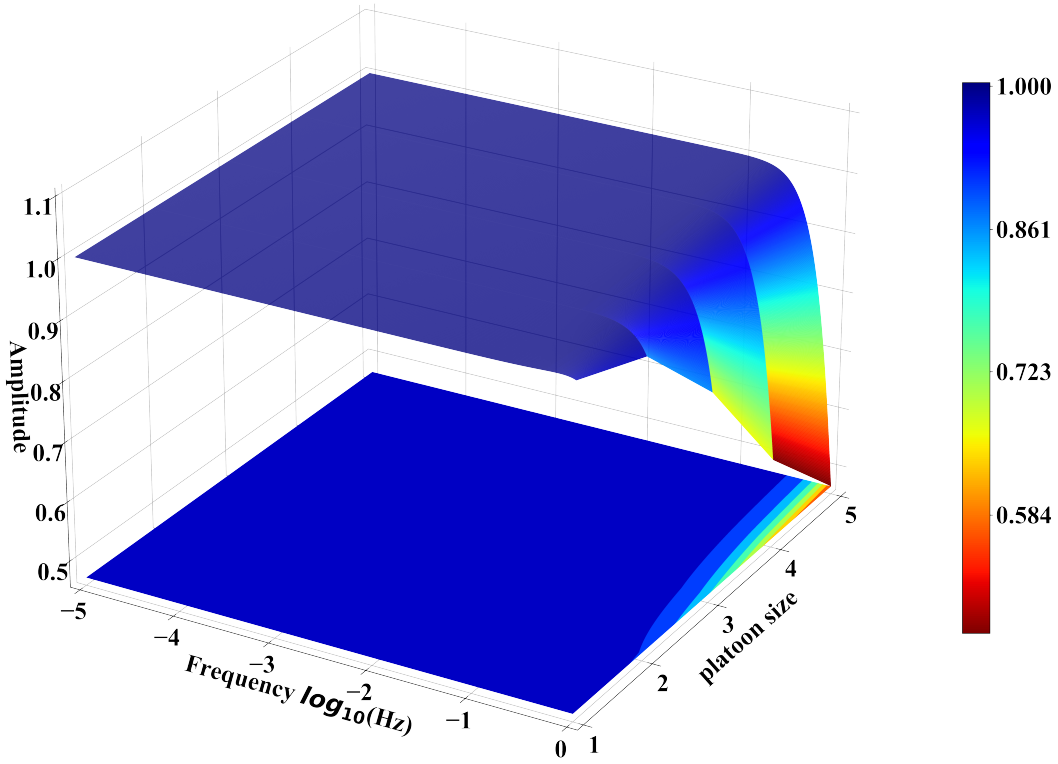


Figure 10 String stability's surface depends on platoon size.

parameterization, a series of simulation experiments are carried out based on CACPC as a supplement to the theoretical analysis.

5.2.1. Simulation experiments maintain a constant speed during the forming and splitting process

Simulation scenario: The simulation scenario is set as follows: at first, a leader vehicle drives on an infinitely long road under a given speed and acceleration configuration (containing five same small perturbations that occurred at the simulation time of 300s, 1000s, 1700s, 2400s, and 3100s under different platoon size). There are four experiments conducted:

1. *Experiment one:* The forming process of the CACC platoon with YK parameterization where an ACC (which is a CACC but degraded to an ACC functionally) follows the leader at the beginning, and more CACCs join the CACC platoon one by one at the simulation time of 700s, 1400s, 2100s, and 2800s.
2. *Experiment two:* The forming process of the CACC platoon without YK parameterization where an ACC (which is a CACC but degraded to an ACC functionally) follows the leader at the beginning, and

more CACCs join the CACC platoon one by one at the simulation time of 700s, 1400s, 2100s, and 2800s.

3. *Experiment three:* The splitting process of the CACC platoon with YK parameterization where an ACC (which is a CACC but degraded to an ACC functionally) follows the leader at the beginning, and more CACCs join the CACC platoon one by one at the simulation time of 700s, 1400s, 2100s, and 2800s.
4. *Experiment four:* The splitting process of the CACC platoon without YK parameterization where an ACC (which is a CACC but degraded to an ACC functionally) and four CACCs follow the leader at the beginning, and the last CACC in the platoon leaves one by one at the simulation time of 700s, 1400s, 2100s, and 2800s.

The first pair of experiments is the forming process of the CACC platoon, where an ACC (which is a CACC but degraded to an ACC functionally) follows the leader at the beginning, and more CACCs join the CACC platoon one by one at the simulation time of 700s, 1400s, 2100s, and 2800s. Moreover, periodic perturbations are applied to the leader to explore the string stability of the CACC platoon under different platoon sizes. Another pair of experiments are conducted simulating the splitting process of the CACC platoon. It should be noted that there are total four experiments conducted to analyze the impact of the YK parameterization under the platoon forming case and the platoon splitting case. Experiment one and three applies YK parameterization with the tuning function γ proposed above, while experiment two and four switch to CACPC mode directly only the platoon size reaches maximum platoon size $S = 5$. Furthermore,

Simulation results. Fig. 11 and 13 show the results of experiments one, two, three and four, respectively. Moreover, Fig. 12 and 14 show the detailed perturbation simulation results of experiments one, two, three and four. In Fig. 11 and 13, (a)-(c) show the simulation results of the case with YK parameterization and (d)-(f) show the simulation results of the case without YK parameterization where (a),(d) Acceleration of simulation results; (b),(e) Velocity of simulation results; (c),(f) Time gap of simulation results. As for Fig. 12 and 14, (a)-(e) show the propagating processes of five applied perturbations and (f)-(i) show the four switching processes of the case with YK parameterization. Furthermore, for the case without YK parameterization, (j)-(n) show the propagating processes of five applied perturbations, and (o)-(r) show the four switching processes.

In Fig. 11 and 12, the process of the gradual formation of the CACC platoon with and without YK parameterization is clearly shown, while the process of the gradual splitting is shown in Fig. 13 and 14. The first attention is spontaneous perturbations during controller switching. From the comparison of Fig. 12 and 14, we can find that the controller switching causes spontaneous perturbations in the process of platoon formation, which is caused by the changing of the equivalent desired time gap. These spontaneous perturbations can be suppressed by applying the tuning function γ to achieve smooth switching. However, in the case without YK parameterization, due to the direct switching when the platoon size reaches or leaves the trigger

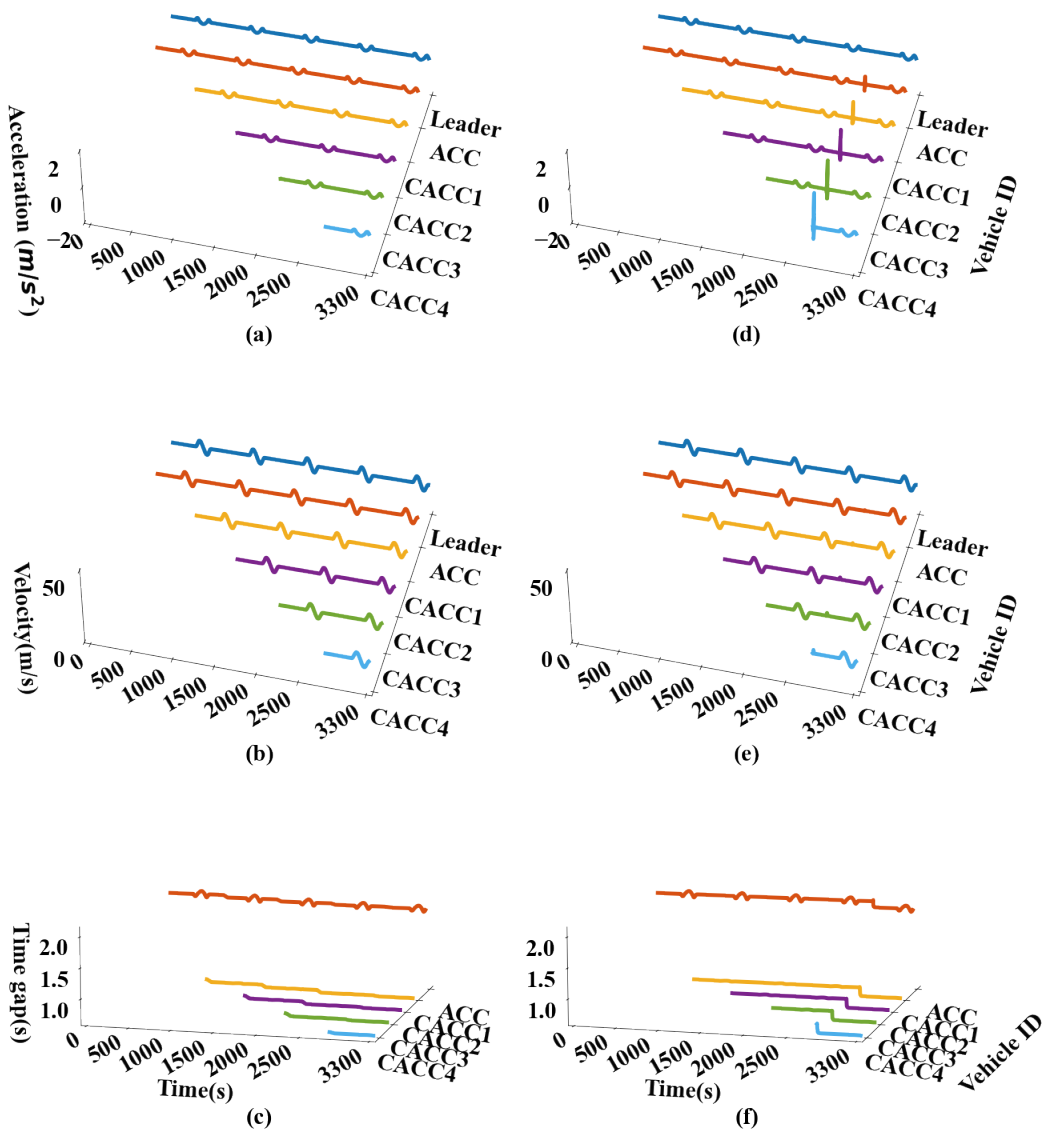


Figure 11 Simulation results of experiment one and two: CACPC with or without YK parameterization under the platoon forming case. (a)-(c) show the simulation results of experiment one, and (d)-(f) show the simulation results of experiment two. (a),(d) Acceleration of simulation results; (b),(e) Velocity of simulation results; (c),(f) Time gap of simulation results.

size, the spontaneous perturbation is too significant, which seriously impacts the stability and safety of the traffic flow. The second attention is string stability. All CACPCs applied under different CACC platoon sizes can maintain string stability through YK parameterization which are shown in Fig. 12 and 14.

Moreover, YK parameterization can work under any CACC MPR since it can be applied even in a typical scenario where the CACC MPR is low and the platoon size is small. Nevertheless, for the case without

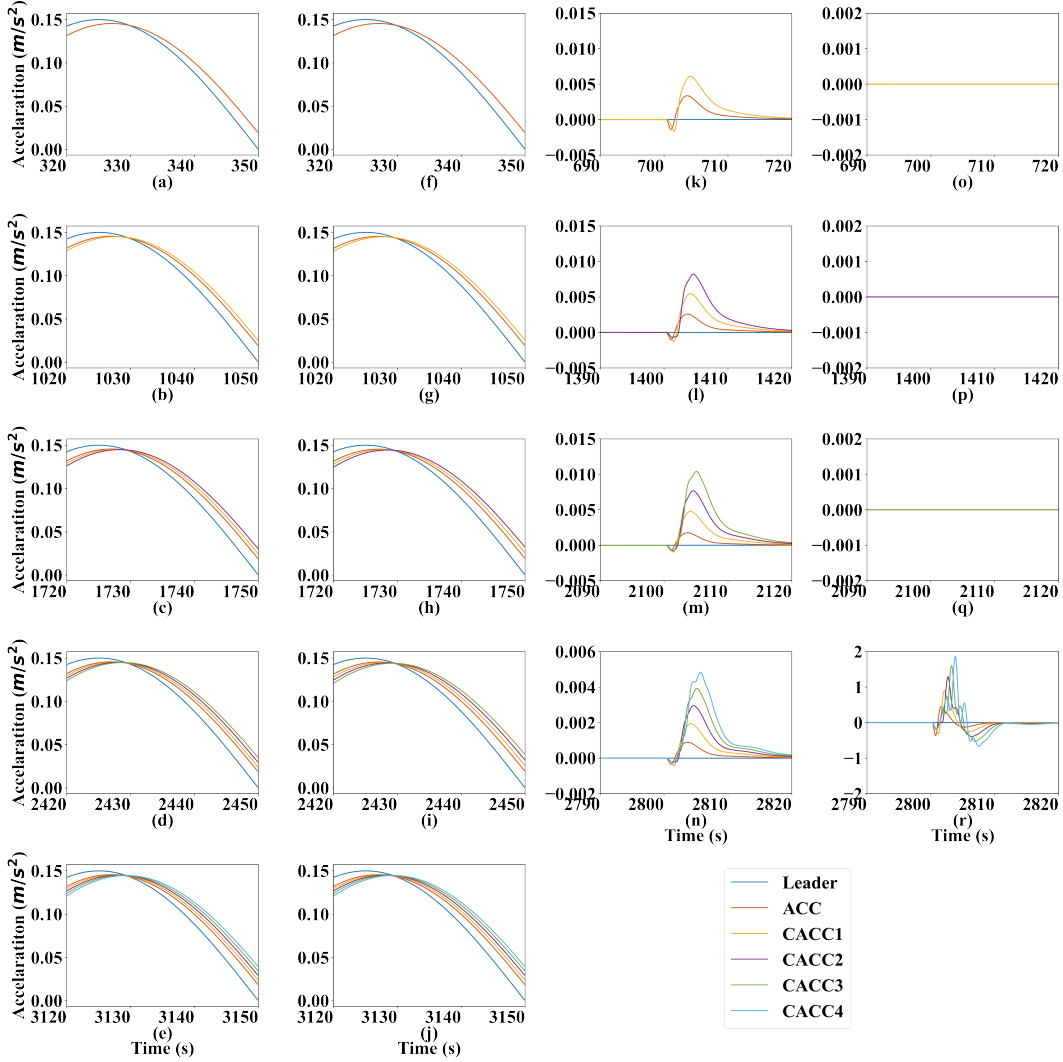


Figure 12 **Detailed perturbation simulation results of experiments one and two: CACPC with or without YK parameterization under the platoon forming case.** For experiment one, (a)-(e) show the propagating processes of five applied perturbations, and (k)-(n) show the four switching processes. For experiment two, (f)-(j) show the propagating processes of five applied perturbations, and (o)-(r) show the four switching processes.

YK parameterization, the CACPCs do not function sufficiently until the set trigger platoon size is reached, which means it is hard to function for a long period because there will be a long time until the CACC MPR gets high. In addition, because the splitting and forming processes are similar, the following simulation experiments are only conducted in the forming process. Notice that from the difference in the acceleration between subplot (a) and (b) in Fig. 11 and 13 which is detailed shown in subplot (k-r) in Fig. 12 and 14, a misunderstood conclusion can be drawn because the perturbation is amplified with or without YK parameterization. However, the perturbation is caused by the equivalent desired time gap increase during the controller switching. In the case with YK parameterization, the perturbation only rises once and then

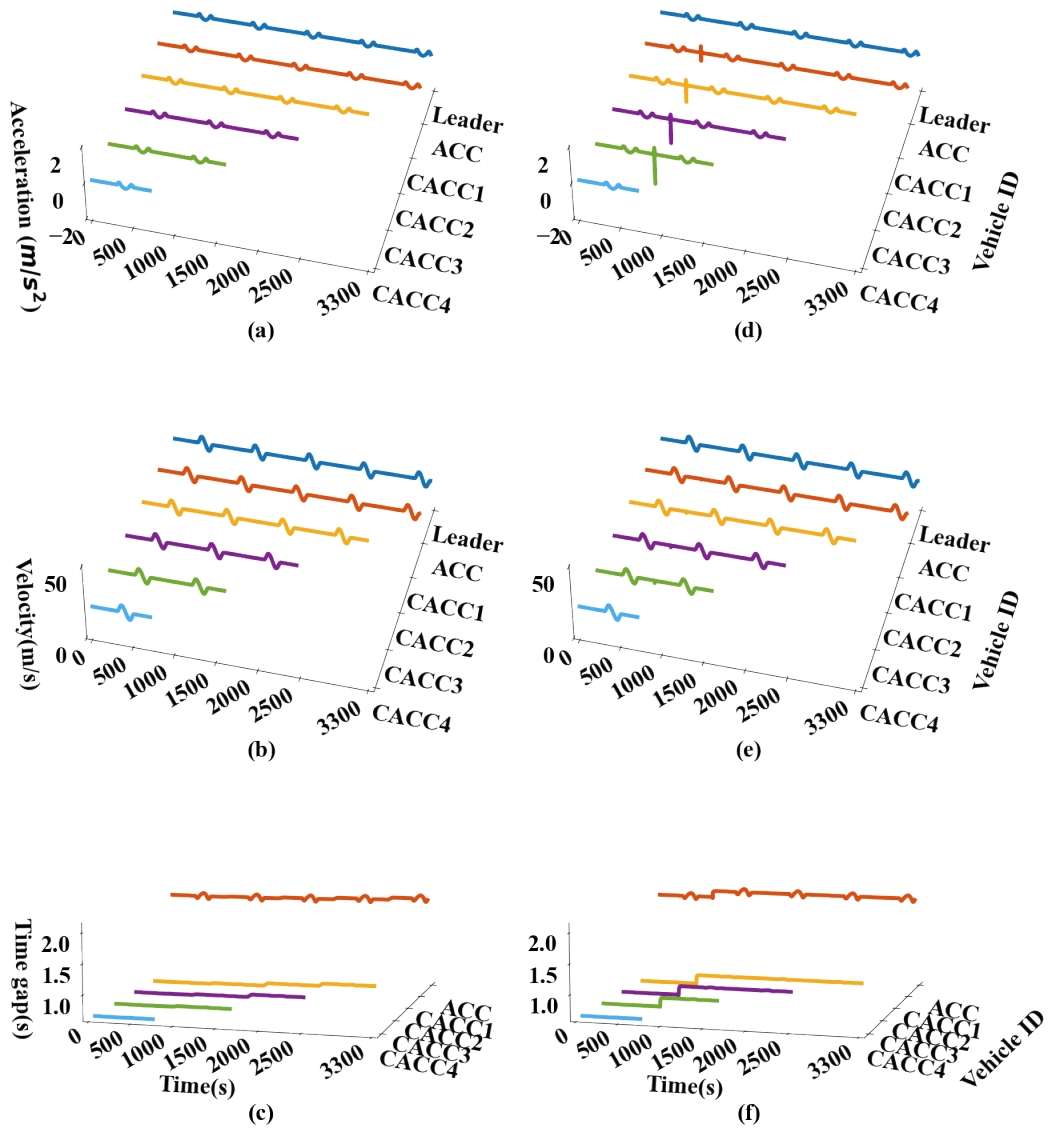


Figure 13 Simulation results of experiments three and four: CACPC with or without YK parameterization under the platoon splitting case. (a)-(c) show the simulation results of experiment three, and (d)-(f) show the simulation results of experiment four. (a),(d) Acceleration of simulation results; (b),(e) Velocity of simulation results; (c),(f) Time gap of simulation results.

back to the equivalent state. Moreover, for the case without YK parameterization, the perturbation fluctuates during the propagating process, which means the switching progress is not smooth enough to suppress the perturbation.

5.2.2. Simulation experiments maintain a fluctuating speed during the forming process *Simulation scenario:* The simulation scenario is similar to experiment one in Section 5.2.1, but different in the given

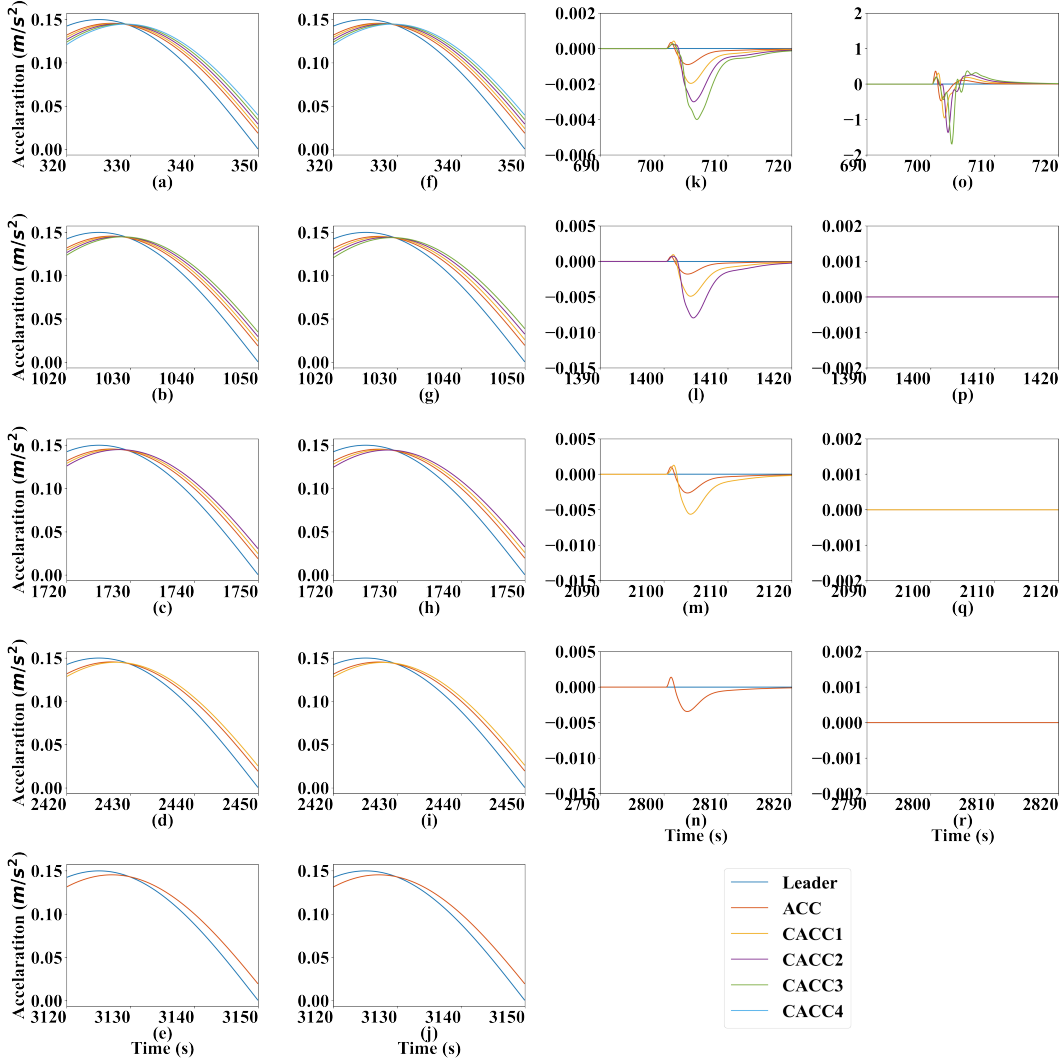


Figure 14 Detailed perturbation simulation results of experiments three and four: CACPC with or without YK parameterization under the platoon splitting case. For experiment three, (a)-(e) show the propagating processes of five applied perturbations, and (k)-(n) show the four switching processes. For experiment four, (f)-(j) show the propagating processes of five applied perturbations, and (o)-(r) show the four switching processes.

speed and acceleration configuration of the leader vehicle. In this simulation experiment, the speed of the leader vehicle fluctuates all the time to simulate the traffic oscillation scenario. There are two experiments conducted:

1. *Experiment five:* The forming process of the CACC platoon with YK parameterization under the fluctuating velocity case where an ACC (which is a CACC but degraded to an ACC functionally) follows the leader at the beginning, and more CACCs join the CACC platoon one by one at the simulation time of 700s, 1400s, 2100s, and 2800s.

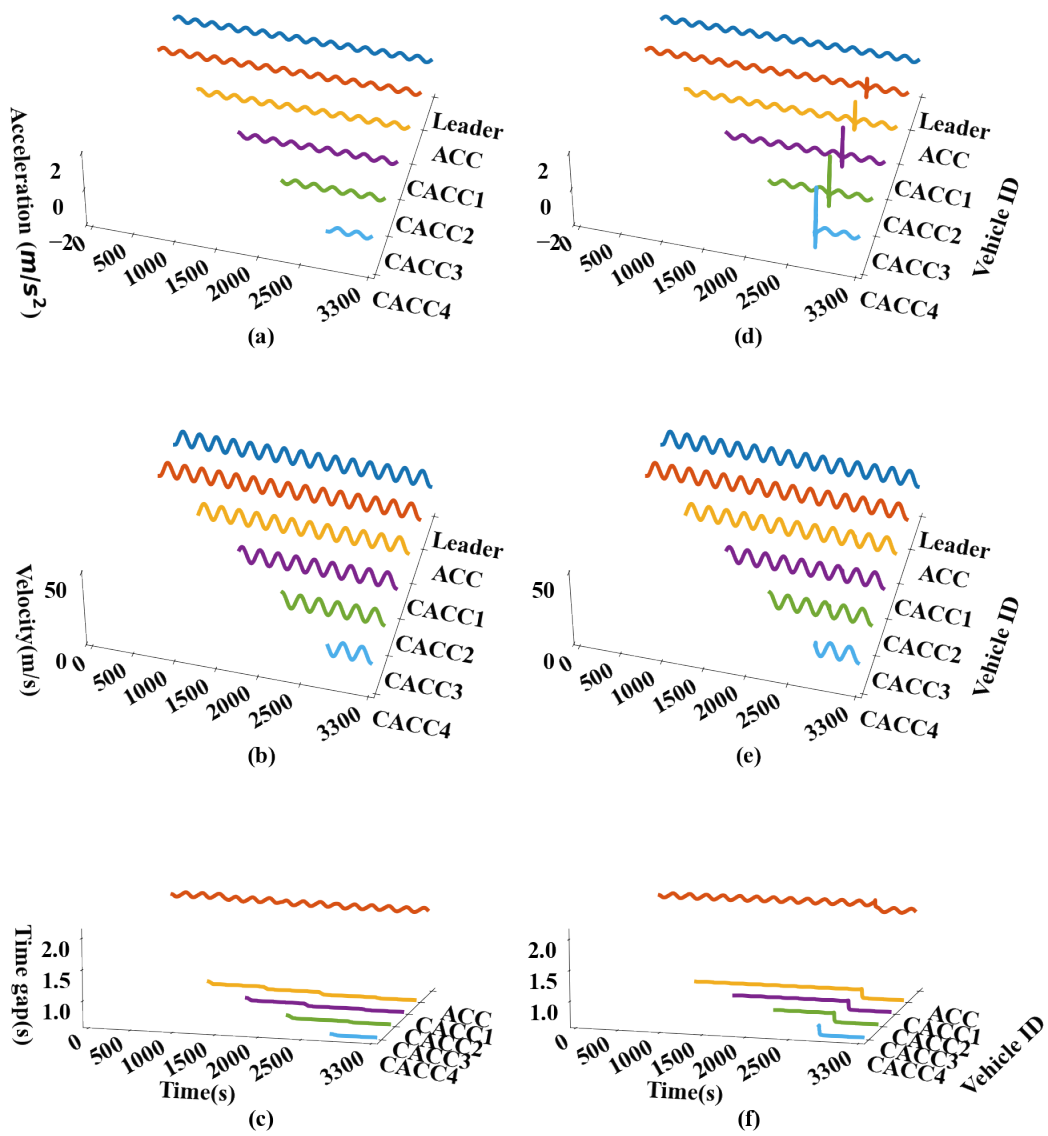


Figure 15 Simulation results of experiments five and six: CACPC with or without YK parameterization under the fluctuating velocity case. (a)-(c) show the simulation results of experiment five, and (d)-(f) show the simulation results of experiment six. (a),(d) Acceleration of simulation results; (b),(e) Velocity of simulation results; (c),(f) Time gap of simulation results.

2. *Experiment six:* The forming process of the CACC platoon without YK parameterization under the fluctuating velocity case where an ACC (which is a CACC but degraded to an ACC functionally) follows the leader at the beginning, and more CACCs join the CACC platoon one by one at the simulation time of 700s, 1400s, 2100s, and 2800s.

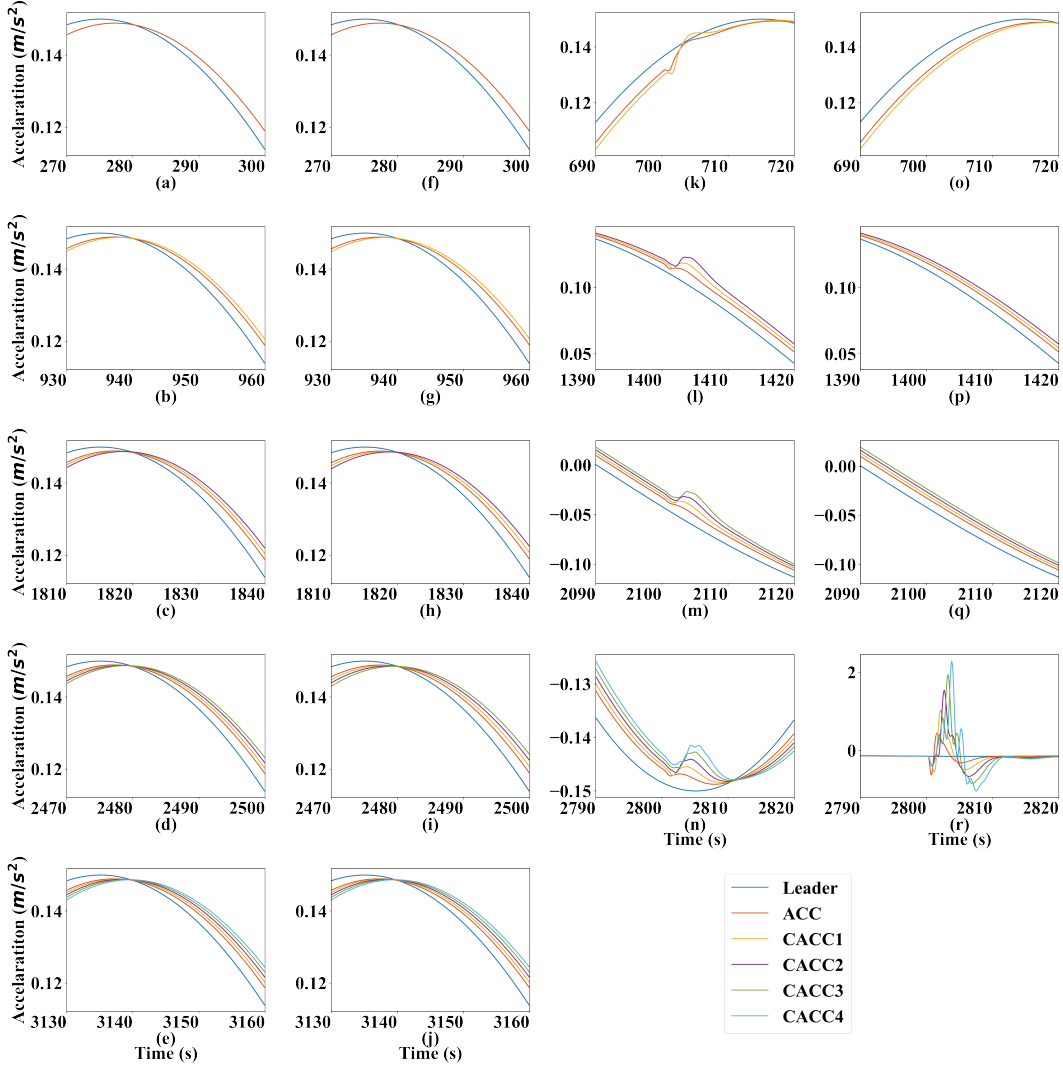


Figure 16 Detailed perturbation simulation results of experiments five and six: CACPC with or without YK parameterization under the fluctuating velocity case. For experiment five, (a)-(e) show the propagating processes of five applied perturbations, and (k)-(l) show the four switching processes. For experiment six, (f)-(j) show the propagating processes of five applied perturbations, and (o)-(r) show the four switching processes.

Simulation results. Fig. 15, 16 show the results of experiments five and six from global and local perspectives, respectively. The formats of Fig. 15, 16 are same as Fig. 11, 12. For the sake of simplicity, the detailed introduction is omitted. In Fig. 15, the top graph plots the vehicles' accelerations, the median graph plots the vehicles' velocities during the simulation, and the bottom graph plots the time gap during the simulation in each figure.

From Fig. 15, the simulation results under the traffic oscillation scenario are similar to the results with constant velocity. The corresponding detailed simulation results are shown in Fig. 16. The spontaneous perturbations caused by the controller switching are not significant and have the magnitude of 0.015 m/s^2

with the YK parameterization, while the perturbation has the magnitude of $2.15 m/s^2$ for the case without YK parameterization under the traffic oscillation scenario. Moreover, a noticeable rise appears in the speed graph, which means a significant negative impact on traffic safety. A conclusion can be drawn that the YK parameterization can ensure the smooth switching of the controllers, whether it is traffic oscillation or equilibrium state.

5.2.3. Simulation experiments maintain a constant speed during the multiple CACCs forming processes *Simulation scenario:* The simulation scenario of experiment seven is set as follows: at first, a leader vehicle drives on an infinitely long road under a given speed and acceleration configuration, which is similar to experiment one in Section 5.2.1. There are only three perturbations at the simulation time of 300s, 1000s and 1700s. Moreover, the forming process of the CACC platoon is that two CACCs join the ACC platoon at the same time, and the forming process repeats twice at the simulation time of 700s and 1400s. Notice that only the case with YK parameterization applied is simulated here because simulation results of the case without YK parameterization are similar to experiment two in Section 5.2.1.

Simulation results. Fig. 17 shows the results of experiment seven. In the left subplot, the top graph plots the vehicles' accelerations, the median graph plots the vehicles' velocities during the simulation, and the bottom graph plots the time gap during the simulation. Moreover, the right subplot shows the detailed acceleration in 690-720s and 1390-1420s to explore the spontaneous perturbation during controllers switching.

From Fig. 17, the first conclusion can be drawn that YK parameterization can keep string stability even during the multiple CACCs forming process. The second conclusion can be found in Fig. 17 (d) and (e) that the spontaneous perturbation caused by controllers switching is amplified with multiple CACCs forming. However, the magnitude of the first switching perturbation is still only $0.015 m/s^2$, which is significantly lower than the case without YK parameterization.

6. Conclusion

This paper proposes a switching control model called CACPC to improve the capability by treating the entire CACC platoon as the control object instead of a single vehicle and switching the control as the platoon size changes. In this control model, the string stability of the CACC platoon is analyzed to obtain the margin time gap for different platoon sizes. Then the YK parameterization is applied to ensure the string stability of the CACC platoon when switching between different control modes, and the corresponding tuning function is proposed so that the application of this control mode is not limited by the fixed platoon size. In addition, the effectiveness of CACPC is explored from two aspects: the effect of YK parameterization on the dynamic performance of CACPC. The following conclusions can be drawn from this paper:

1. A new switching control mode is proposed to control the whole CACC platoon instead of a single vehicle.

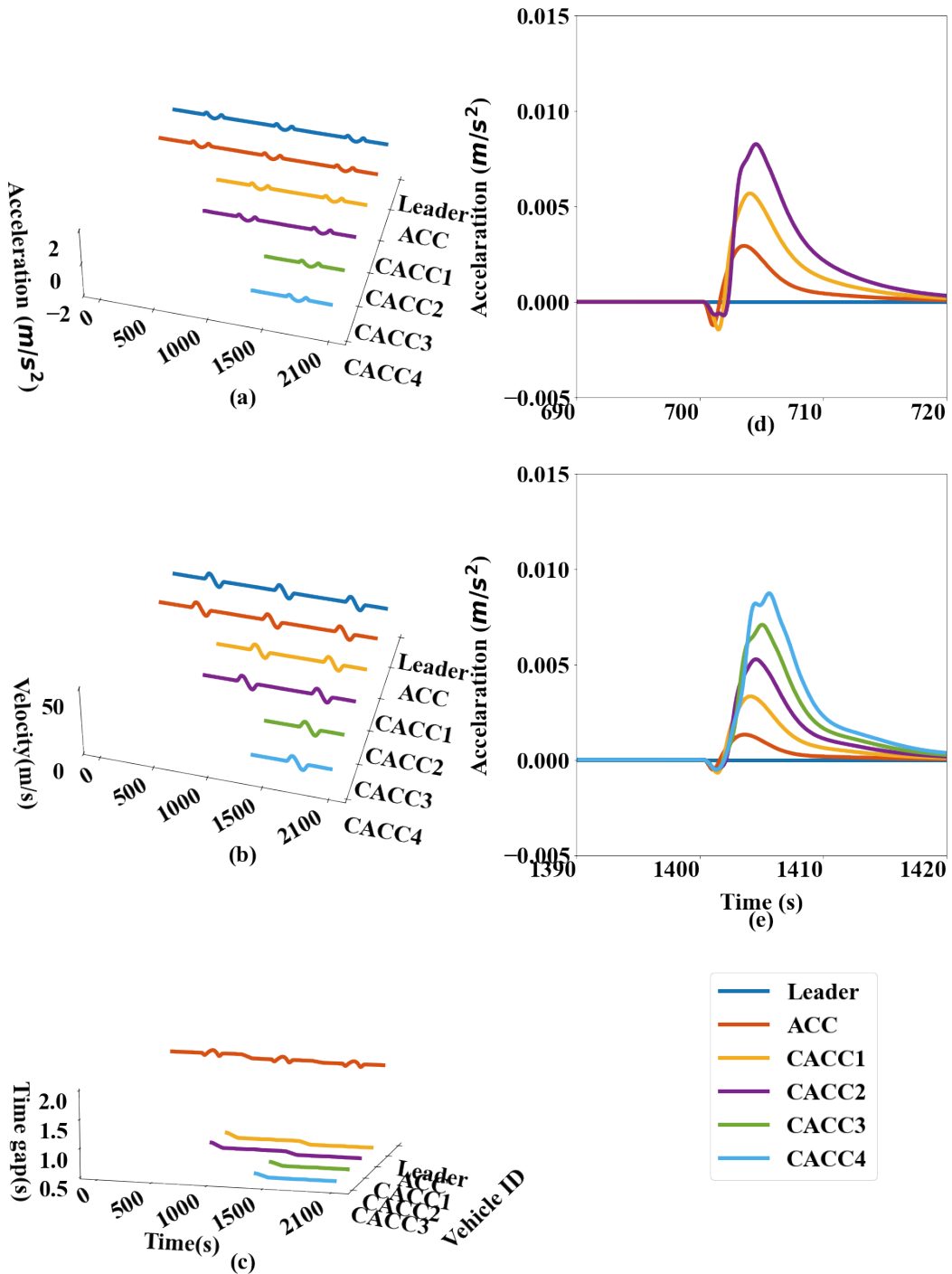


Figure 17 Simulation results of experiment seven: CACPC with YK parameterization under multiple CACCs forming at the same time. (a) Acceleration of simulation results; (b) Velocity of simulation results; (c) Time gap of simulation results; (d) Detailed acceleration of simulation results in 690-720s; (e) Detailed acceleration of simulation results in 1390-1420s

Table 2 Parameters chosen for different experiment groups.

Index of experiments group	k_p	k_d	h_i	round
1 st	0.7s^{-2}	0s^{-1}	2 s	2
2 nd	0.5s^{-2}	0s^{-1}	1.8 s	5
3 rd	0.6s^{-2}	0s^{-1}	2 s	7
4 th	0.7s^{-2}	0s^{-1}	2 s	4
5 th	0.4s^{-2}	0s^{-1}	2 s	3

2. CACPC consists of two sets of CACC controllers. YK parameterization ensures stable coupling between the two sets of controllers to guarantee smooth switching and string stability at different platoon sizes.
3. Combination of tuning function γ under different platoon sizes is derived by ensuring that the application range of CACPC is not limited by platoon size.
4. Adopting YK parameterization can significantly suppress the spontaneous perturbation from $2m/s^2$ to $0.015m/s^2$ caused by the controller switch.
5. YK parameterization can ensure smooth controller switching under the equilibrium state, traffic oscillation, and multiple CACCs forming.

Acknowledgments

This research was sponsored by the National Key Research and Development Program of China (No. 2019YFB1600200), National Science Foundation of China (No. 51878161, No. 71931002 and No.52072067).

Appendix A: System identification of lower level controller based on field experiments

Experiment preparation: The experiment was conducted at Closed test site of National Smart CAV & C-ITS (Beijing + Hebei) Demonstration Zone Shunyi Base on March 29, 2021. Two cycabs were used for experiment which were autonomous driving vehicles developed by iDriverplus technology company. The scheme of LiDAR+ millimeter wave + Ultrasonic radar + GPS inertial navigation was adopted as the navigation system, and the distance measurement accuracy is 0.05m. The decision frequency is 20 Hz which equals to a 50ms decision interval. The Fig. 18 show the scene of the field experiment.

Experiment scheme: The experiments was divided into 5 groups. Each group had several rounds, which amounted to a total of 21 rounds of experiments. In each round, the front car drove in accordance with the speed configuration while the back car used the longitudinal control of ACC system to follow the front car and recorded the actual acceleration of the back car. Different groups used different control parameters of ACC system to ensure that a general conclusion can be drawn.

The control parameters of ACC system in different experiment groups are shown in communication, the specific parameter setting is shown in Table. 2.

The experiment data of command acceleration and actual acceleration in first round are shown in Fig. 19, where a_{cmd} means the command acceleration and a_{actual} means the actual acceleration.

In order to calibrate the transfer function of the lower controller $G_s(s)$, the command acceleration and actual acceleration of the back car in each round are regarded as input and output respectively. Notice that since the output of



Figure 18 Field experiment scene.

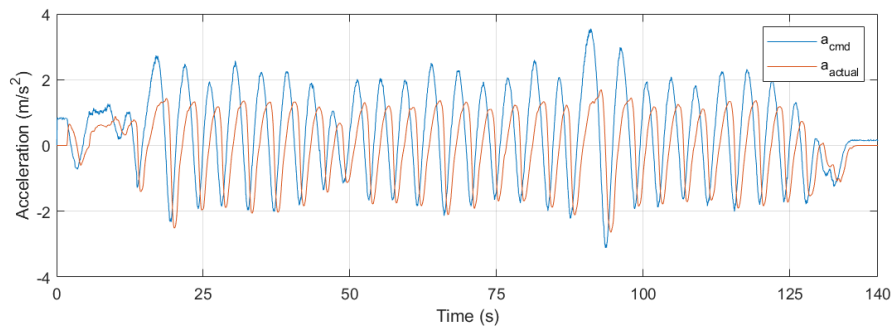


Figure 19 Experiment data of the command acceleration and the actual acceleration in first round, where a_{cmd} means the command acceleration and a_{actual} means the actual acceleration.

the lower controller $G_s(s)$ in Fig. 2 is position instead of acceleration, additional second-order integration is applied. Using the System Identification toolbox in MATLAB and setting desire system type, the transfer function is fitted as

follows:

$$G_i(s) = \frac{k_G}{s^2(\tau_i s + 1)} e^{-\phi_i s} = \frac{0.9403}{s^2(0.7862s + 1)} e^{-0.2s}, \quad (31)$$

which keeps fit error to minimum: FPE=0.08699 and MSE=0.0868.

Appendix B: Proof of the Equation (17-18)

The Equation (17-18) must satisfy the following identities:

$$1. \quad G = NM^{-1} = \tilde{M}^{-1}\tilde{N},$$

$$2. \quad K_i = U_i V_i^{-1} = \tilde{V}_i^{-1} \tilde{U}_i,$$

$$3. \quad \begin{bmatrix} \tilde{V}_i & -\tilde{U}_i \\ -\tilde{N} & \tilde{M} \end{bmatrix} \begin{bmatrix} M & U_i \\ N & V_i \end{bmatrix} = \begin{bmatrix} M & U_i \\ N & V_i \end{bmatrix} \begin{bmatrix} \tilde{V}_i & -\tilde{U}_i \\ -\tilde{N} & \tilde{M} \end{bmatrix} = \begin{bmatrix} I & 0 \\ 0 & I \end{bmatrix}.$$

Proof. Proof of (a) $G = \tilde{M}^{-1}\tilde{N}$:

$$\begin{aligned} & \tilde{M}^{-1}\tilde{N} \\ &= \left[\begin{array}{cc|c} A + BD_i^c C & BC_i^c & BD_i^c \\ B_i^c C & A_i^c & B_i^c \\ \hline C & -F_i^c & I \end{array} \right]^{-1} \left[\begin{array}{cc|c} A + BD_i^c C & BC_i^c & B \\ B_i^c C & A_i^c & 0 \\ \hline C & -F_i^c & 0 \end{array} \right] \\ &= \left[\begin{array}{cc|c} A & B(C_i^c + D_i^c F_i^c) & -BD_i^c \\ 0 & A_i^c + B_i^c F_i^c & -B_i^c \\ \hline C & -F_i^c & I \end{array} \right] \left[\begin{array}{cc|c} A + BD_i^c C & BC_i^c & B \\ B_i^c C & A_i^c & 0 \\ \hline C & -F_i^c & 0 \end{array} \right] \\ &= \left[\begin{array}{cc|c} A & B(C_i^c + D_i^c F_i^c) & -BD_i^c C & BD_i^c F_i^c \\ 0 & A_i^c + B_i^c F_i^c & -B_i^c C & B_i^c F_i^c \\ 0 & 0 & A + BD_i^c C & BC_i^c \\ 0 & 0 & B_i^c C & A_i^c \\ \hline C & -F_i^c & C & -F_i^c \end{array} \right] \left[\begin{array}{c|c} 0 & B \\ 0 & 0 \\ \hline 0 & 0 \end{array} \right] \\ &= \left[\begin{array}{cc|c} A & B(C_i^c + D_i^c F_i^c) & 0 & 0 \\ 0 & A_i^c + B_i^c F_i^c & 0 & 0 \\ 0 & 0 & A + BD_i^c C & BC_i^c \\ 0 & 0 & B_i^c C & A_i^c \\ \hline C & -F_i^c & 0 & 0 \end{array} \right] \left[\begin{array}{c|c} B & 0 \\ 0 & 0 \\ \hline 0 & 0 \end{array} \right] \\ &= \left[\begin{array}{c|c} A & B \\ C & 0 \end{array} \right], \end{aligned} \quad (32)$$

where $\mathbf{T} = \begin{bmatrix} \mathbf{I} & 0 & -\mathbf{I} & 0 \\ 0 & \mathbf{I} & 0 & -\mathbf{I} \\ 0 & 0 & \mathbf{I} & 0 \\ 0 & 0 & 0 & \mathbf{I} \end{bmatrix}$, $\mathbf{T}^{-1} = \begin{bmatrix} \mathbf{I} & 0 & \mathbf{I} & 0 \\ 0 & \mathbf{I} & 0 & \mathbf{I} \\ 0 & 0 & \mathbf{I} & 0 \\ 0 & 0 & 0 & \mathbf{I} \end{bmatrix}$ is adopted in the similarity transformation. The proofs that $G = NM^{-1}$ and (ii) are analogous.

$$\text{Proof.} \quad \text{Proof of (c)} \quad \begin{bmatrix} M & U_i \\ N & V_i \end{bmatrix} \begin{bmatrix} \tilde{V}_i & -\tilde{U}_i \\ -\tilde{N} & \tilde{M} \end{bmatrix} = \begin{bmatrix} I & 0 \\ 0 & I \end{bmatrix}.$$

$$\begin{aligned}
& \begin{bmatrix} M & U_i \\ N & V_i \end{bmatrix}^{-1} \\
&= \begin{bmatrix} A + BF & 0 & -B & 0 \\ 0 & A_i^c + B_i^c F_i^c & 0 & B_i^c \\ -F & C_i^c + D_i^c F_i^c & I & D_i^c \\ -C & F_i^c & 0 & I \end{bmatrix}^{-1} \\
&= \begin{bmatrix} A + BD_i^c C & BC_i^c & -B & BD_i^c \\ B_i^c C & A_i^c & 0 & B_i^c \\ F_i - D_i^c C & -C_i^c & I & -D_i^c \\ C & -F_i^c & 0 & I \end{bmatrix} \\
&= \begin{bmatrix} \tilde{V}_i & -\tilde{U}_i \\ -\tilde{N} & \tilde{M} \end{bmatrix}.
\end{aligned} \tag{33}$$

Q.E.D.

References

- Bansal P, Kockelman KM, 2017 *Forecasting Americans' long-term adoption of connected and autonomous vehicle technologies*. *Transportation Research Part A: Policy and Practice* 95:49–63.
- Bian Y, Zheng Y, Ren W, Li SE, Wang J, Li K, 2019 Reducing time headway for platooning of connected vehicles via v2v communication. *Transportation Research Part C: Emerging Technologies* 102:87–105.
- Darbha S, 2003 *On the synthesis of controllers for continuous time LTI systems that achieve a non-negative impulse response*. *Automatica* 39(1):159–165.
- Dasgupta S, Anderson BD, 1996 A parametrization for the closed-loop identification of nonlinear time-varying systems. *Automatica* 32(10):1349–1360.
- Dey KC, Yan L, Wang X, Wang Y, Shen H, Chowdhury M, Yu L, Qiu C, Soundararaj V, 2015 A review of communication, driver characteristics, and controls aspects of cooperative adaptive cruise control (cacc). *IEEE Transactions on Intelligent Transportation Systems* 17(2):491–509.
- Feng S, Zhang Y, Li SE, Cao Z, Liu HX, Li L, 2019 String stability for vehicular platoon control: Definitions and analysis methods. *Annual Reviews in Control* 47:81–97.
- Gong S, Du L, 2018 Cooperative platoon control for a mixed traffic flow including human drive vehicles and connected and autonomous vehicles. *Transportation research part B: methodological* 116:25–61.
- Jin IG, Orosz G, 2014 Dynamics of connected vehicle systems with delayed acceleration feedback. *Transportation Research Part C: Emerging Technologies* 46:46–64.
- Mahtout I, Navas F, Milanes V, Nashashibi F, 2020 Advances in youla-kucera parametrization: A review. *Annual Reviews in Control* 49:81–94.
- Marsden G, McDonald M, Brackstone M, 2001 Towards an understanding of adaptive cruise control. *Transportation Research Part C: Emerging Technologies* 9(1):33–51.
- Milanés V, Shladover SE, 2014 Modeling cooperative and autonomous adaptive cruise control dynamic responses using experimental data. *Transportation Research Part C: Emerging Technologies* 48:285–300.

- Milanés V, Shladover SE, Spring J, Nowakowski C, Kawazoe H, Nakamura M, 2013 *Cooperative adaptive cruise control in real traffic situations*. *IEEE Transactions on intelligent transportation systems* 15(1):296–305.
- Montanino M, Monteil J, Punzo V, 2021 *From homogeneous to heterogeneous traffic flows: Lp string stability under uncertain model parameters*. *Transportation Research Part B: Methodological* 146:136–154.
- Montanino M, Punzo V, 2021a *On string stability of a mixed and heterogeneous traffic flow: A unifying modelling framework*. *Transportation Research Part B: Methodological* 144:133–154, URL <http://dx.doi.org/10.1016/j.trb.2020.11.009>, publisher: Elsevier Ltd.
- Montanino M, Punzo V, 2021b *On string stability of a mixed and heterogeneous traffic flow: A unifying modelling framework*. *Transportation Research Part B: Methodological* 144:133–154.
- Naus GJ, Vugts RP, Ploeg J, van De Molengraft MJ, Steinbuch M, 2010 *String-stable cacc design and experimental validation: A frequency-domain approach*. *IEEE Transactions on vehicular technology* 59(9):4268–4279.
- Navas F, Milanés V, 2019 *Mixing v2v-and non-v2v-equipped vehicles in car following*. *Transportation research part C: emerging technologies* 108:167–181.
- Navas F, Milanés V, Nashashibi F, 2016 *Using plug&play control for stable acc-cacc system transitions*. *2016 IEEE Intelligent Vehicles Symposium (IV)*, 704–709 (IEEE).
- Navas F, Milanés V, Nashashibi F, 2017 *Youla-kucera based online closed-loop identification for longitudinal vehicle dynamics*. *2017 21st International Conference on System Theory, Control and Computing (ICSTCC)*, 88–93 (IEEE).
- Niemann H, Stoustrup J, 1999 *An architecture for implementation of multivariable controllers*. *Proceedings of the 1999 American Control Conference (Cat. No. 99CH36251)*, volume 6, 4029–4033 (IEEE).
- Oncu S, Ploeg J, Van De Wouw N, Nijmeijer H, 2014 *Cooperative adaptive cruise control: Network-aware analysis of string stability*. *IEEE Transactions on Intelligent Transportation Systems* 15(4):1527–1537, URL <http://dx.doi.org/10.1109/TITS.2014.2302816>.
- Orosz Gb, Moehlis J, Bullo F, 2011 *Delayed car-following dynamics for human and robotic drivers*. *International Design Engineering Technical Conferences and Computers and Information in Engineering Conference*, volume 54815, 529–538.
- Ploeg J, Scheepers BT, Van Nunen E, Van de Wouw N, Nijmeijer H, 2011 *Design and experimental evaluation of cooperative adaptive cruise control*. *2011 14th International IEEE Conference on Intelligent Transportation Systems (ITSC)*, 260–265 (IEEE).
- Ploeg J, Van De Wouw N, Nijmeijer H, 2013 *Lp string stability of cascaded systems: Application to vehicle platooning*. *IEEE Transactions on Control Systems Technology* 22(2):786–793.
- Pommaret J, Quadrat A, 1998 *Generalized bezout identity*. *Applicable Algebra in Engineering, Communication and Computing* 9(2):91–116.
- Qin Y, Wang H, 2021 *Analytical framework of string stability of connected and autonomous platoons with electronic throttle angle feedback*. *Transportmetrica A: Transport Science* 17(1):59–80.

- Qin Y, Wang H, Ni D, 2021 *Lighthill-Whitham-Richards Model for Traffic Flow Mixed with Cooperative Adaptive Cruise Control Vehicles*. *Transportation Science* 55(4):883–907, URL <http://dx.doi.org/10.1287/trsc.2021.1057>.
- Qin Y, Wang H, Ran B, 2018 *Stability analysis of connected and automated vehicles to reduce fuel consumption and emissions*. *Journal of Transportation Engineering, Part A: Systems* 144(11):04018068.
- Ruan T, Wang H, Zhou L, Zhang Y, Dong C, Zuo Z, 2022 *Impacts of Information Flow Topology on Traffic Dynamics of CAV-MV Heterogeneous Flow*. *IEEE Transactions on Intelligent Transportation Systems* 1–16, URL <http://dx.doi.org/10.1109/TITS.2022.3170965>.
- Ruan T, Zhou L, Wang H, 2021 *Stability of heterogeneous traffic considering impacts of platoon management with multiple time delays*. *Physica A: Statistical Mechanics and its Applications* 583:126294.
- Shang M, Stern RE, 2021 *Impacts of commercially available adaptive cruise control vehicles on highway stability and throughput*. *Transportation Research Part C: Emerging Technologies* 122:102897, URL <http://dx.doi.org/10.1016/j.trc.2020.102897>, publisher: Pergamon.
- Shen J, Kammara EKH, Du L, 2021 *Fully Distributed Optimization based CAV Platooning Control under Linear Vehicle Dynamics*. ArXiv:2103.11081 [math].
- Stefanovic M, Safonov MG, 2008 *Safe Adaptive Switching Control: Stability and Convergence*. *IEEE Transactions on Automatic Control* 53(9):2012–2021, URL <http://dx.doi.org/10.1109/TAC.2008.929395>.
- Stüdli S, Seron MM, Middleton RH, 2017 *From vehicular platoons to general networked systems: String stability and related concepts*. *Annual Reviews in Control* 44:157–172.
- Stüdli S, Seron MM, Middleton RH, 2017 *From vehicular platoons to general networked systems: String stability and related concepts*. *Annual Reviews in Control* 44(2):157–172, URL <http://dx.doi.org/10.1016/j.arcontrol.2017.09.016>.
- Sun J, Zheng Z, Sun J, 2018 *Stability analysis methods and their applicability to car-following models in conventional and connected environments*. *Transportation research part B: methodological* 109:212–237.
- Swaroop D, 1994 *String stability of interconnected systems: An application to platooning in automated highway systems*.
- Tay TT, Mareels I, Moore JB, 1998 *High performance control* (Springer Science & Business Media).
- Verizon North LLC, 2020 *Federal Communications Commission. Proceeding Number* 19:354.
- Wang C, Gong S, Zhou A, Li T, Peeta S, 2020 *Cooperative adaptive cruise control for connected autonomous vehicles by factoring communication-related constraints*. *Transportation Research Part C: Emerging Technologies* 113:124–145.
- Wang J, Lu L, Peeta S, 2022 *Real-time deployable and robust cooperative control strategy for a platoon of connected and autonomous vehicles by factoring uncertain vehicle dynamics*. *Transportation Research Part B: Methodological* 163:88–118, URL <http://dx.doi.org/10.1016/j.trb.2022.06.012>.

- Wang M, 2018 *Infrastructure assisted adaptive driving to stabilise heterogeneous vehicle strings*. *Transportation Research Part C: Emerging Technologies* 91:276–295.
- Wang Z, Bian Y, Shladover SE, Wu G, Li SE, Barth MJ, 2019 *A survey on cooperative longitudinal motion control of multiple connected and automated vehicles*. *IEEE Intelligent Transportation Systems Magazine* 12(1):4–24.
- Xiao L, Gao F, 2011 *Practical string stability of platoon of adaptive cruise control vehicles*. *IEEE Transactions on intelligent transportation systems* 12(4):1184–1194.
- Xu L, Zhuang W, Yin G, Bian C, 2019 *Energy-oriented cruising strategy design of vehicle platoon considering communication delay and disturbance*. *Transportation Research Part C: Emerging Technologies* 107:34–53, URL <http://dx.doi.org/10.1016/j.trc.2019.07.019>.
- Yao Z, Xu T, Jiang Y, Hu R, 2021 *Linear stability analysis of heterogeneous traffic flow considering degradations of connected automated vehicles and reaction time*. *Physica A: Statistical Mechanics and its Applications* 561.
- Zhang Y, Bai Y, Hu J, Wang M, 2020 *Control design, stability analysis, and traffic flow implications for cooperative adaptive cruise control systems with compensation of communication delay*. *Transportation Research Record* 2674(8):638–652.
- Zhou L, Ruan T, Ma K, Dong C, Wang H, 2021 *Impact of cav platoon management on traffic flow considering degradation of control mode*. *Physica A: Statistical Mechanics and its Applications* 126193.
- Zhou Y, Ahn S, Wang M, Hoogendoorn S, 2020 *Stabilizing mixed vehicular platoons with connected automated vehicles: An h-infinity approach*. *Transportation Research Part B: Methodological* 132:152–170.